

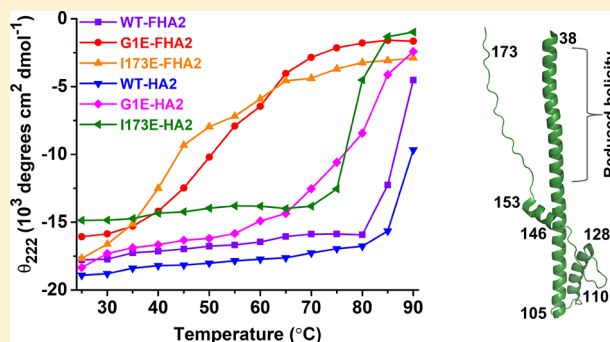
The Stabilities of the Soluble Ectodomain and Fusion Peptide Hairpins of the Influenza Virus Hemagglutinin Subunit II Protein Are Positively Correlated with Membrane Fusion

Ahinsa Ranaweera, Punsisi U. Ratnayake, and David P. Weliky*¹

Department of Chemistry, Michigan State University, East Lansing, Michigan 48824, United States

S Supporting Information

ABSTRACT: Cellular entry of influenza virus is mediated by the viral protein hemagglutinin (HA), which forms an initial complex of three HA1 and three HA2 subunits. Each HA2 includes a fusion peptide (FP), a soluble ectodomain (SE), and a transmembrane domain. HA1 binds to cellular sialic acids, followed by virus endocytosis, pH reduction, dissociation of HA1, and structural rearrangement of HA2 into a final trimer-of-SE hairpins. A decrease in pH also triggers HA2-mediated virus/endosome membrane fusion. SE hairpins have an interior parallel helical bundle and C-terminal strands in the grooves of the exterior of the bundle. FPs are separate helical hairpins. This study compares wild-type HA2 (WT-HA2) with G1E(FP) and I173E(SE strand) mutants. WT-HA2 induces vesicle fusion at pH 5.0, whereas the extent of fusion is greatly reduced for both mutants.



Circular dichroism for HA2 and FHA2≡FP+SE constructs shows dramatic losses of stability for the mutants, including a T_m reduced by 40 °C for I173E-FHA2. This is evidence of destabilization of SE hairpins via dissociation of strands from the helical bundle, which is also supported by larger monomer fractions for mutant versus WT proteins. The G1E mutant may have disrupted FP hairpins, with consequent non-native FP binding to dissociated SE strands. It is commonly proposed that free energy released by the HA2 structural rearrangement catalyzes HA-mediated fusion. This study supports an alternate mechanistic model in which fusion is preceded by FP insertion in the target membrane and formation of the final SE hairpin. Less fusion by the mutants is due to the loss of hairpin stability and consequent reduced level of membrane apposition of the virus and target membranes.

Influenza is an enveloped RNA virus in the family Orthomyxoviridae and is either spherical with an ~100 nm diameter or filamentous with an ~300 nm length.¹ An initial infection step is fusion (joining) of the virus and cell membranes with consequent deposition of the nucleocapsid in the host cytoplasm.^{2–4} The influenza virus hemagglutinin (HA) protein mediates binding of the virus to the host cell and subsequent membrane fusion. HA is translated as a single protein and then proteolytically cleaved into the disulfide-linked subunits HA1 (328 residues) and HA2 (221 residues). Fusion is catalyzed by HA2, which contains the fusion peptide (FP), the soluble ectodomain (SE), the transmembrane domain (TM), and the endodomain (~25, 160, 25, and 10 residues, respectively) (Figure 1). The initial HA complex outside the membrane includes three HA2 ectodomains and three HA1's. The complex has a mushroom shape with a stem (HA2 trimer) and a head (HA1's).^{5,6} The stem includes an interior core with a parallel coiled coil of residue 76–125 helices. The HA2 N-terminal regions include 56–75 extended loops, 38–55 helices that pack antiparallel in exterior grooves of the coiled coil, and 1–20 irregular FP and 21–35 antiparallel β -sheet structures located between the stem and the head. The C-terminal HA2 regions include 130–141 β -

sheet hairpins and compactly associated 146–153 and 159–170 helices.

Host cell infection begins with binding of HA1 to cell-surface sialic acids, which initiates endocytosis and then endosome maturation with a decrease in pH to <6. HA1 separates from HA2 at this pH, and the HA2 SE transforms to a final-state trimer-of-hairpins structure (Figure 1B).^{7,8} This structure includes an interior core of parallel coiled-coil 38–105 helices, 106–109 180° turns, and 110–128 helices and 154–176 strands that both pack antiparallel in the exterior grooves of the coiled coil. Structural differences between the initial and final SE states include (1) the 38–55 exterior helices and 56–75 loops becoming part of the interior helices, (2) the 106–128 interior helices becoming the 106–109 turns and 110–128 exterior helices, and (3) the 159–170 helices becoming part of the 154–176 strand regions of the hairpins.

Besides causing significant HA structural rearrangement, the reduced pH is also the trigger for virus/endosome membrane fusion. Most mechanistic insight into fusion is based on the

Received: July 17, 2018

Revised: August 23, 2018

Published: August 24, 2018

(A) FHA2 sequence

1 GLFGAIAGFIENGWEGMIDGWYGRHQNSEGTGQAADLKSTQAAIDQING
 51 KLNRVIEKTNEKFHQIEKEFSEVEGRIQDLEKYVEDTKIDLWSYNAELLV
 101 ALENQHTIDLTDSEMKNLFKFKTRRQLRENAEEMGNFSFKIYHKADNAAE
 151 SIRNGTYDHDVYRDEALNRRFQIKGVLEKSGYKDWLEHHHHHH

HA2 sequence

1 GLFGAIAGFIENGWEGMIDGWYGRHQNSEGTGQAADLKSTQAAIDQING
 51 KLNRVIEKTNEKFHQIEKEFSEVEGRIQDLEKYVEDTKIDLWSYNAELLV
 101 ALENQHTIDLTDSEMKNLFKFKTRRQLRENAEEMGNFSFKIYHKADNAAE
 151 SIRNGTYDHDVYRDEALNRRFQIKGVLEKSGYKDWILWISFAISAFLLAV
 201 VLLGFIMWAAQRGNIRANIAIGGGGGLEHHHHHH

(B) Fusion peptide and soluble ectodomain structures

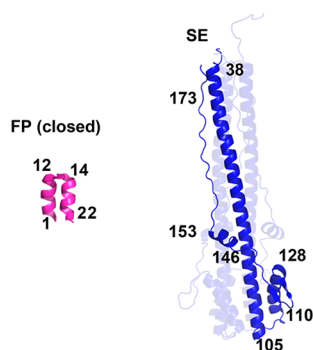


Figure 1. (A) Amino acid sequences of the FHA2 and HA2 constructs with colored domains: fusion peptide (FP), pink; soluble ectodomain (SE), blue; transmembrane domain (TM), green; and endodomain, orange. The non-native C-terminal regions (black) include a H_6 tag for affinity chromatography. The underlined residues denote the sites of the G1E and I173E mutations. (B) Ribbon diagrams of the FP in the closed conformation [Protein Data Bank (PDB) entry 2KXA] and trimeric SE in the final hairpin conformation (PDB entry 1QU1).

surrogate system of fusion between HA-expressing cells (HA cells) and red blood cells (RBC's). The process includes a hemifusion step with outer leaflet membrane mixing, followed by breakage of the hemifusion diaphragm by pore formation, and then pore expansion.^{9–11} There hasn't yet been imaging that temporally correlates the HA structural changes and membrane changes during fusion, so mechanisms are primarily based on effects of mutations on fusion.^{10,12,13}

The HA2 FP is sequestered in the interior of the initial HA complex and is released during the process of HA1/HA2 separation and HA2 structural transformation into the final hairpin state. The FP is the most conserved region of the HA sequence and is important in all steps of membrane fusion, as evidenced by both the G1E mutant (HA2 numbering), which results in no HA cell/RBC fusion, and the G1S mutant, which results in hemifusion without pore expansion.^{10,14,15} The nuclear magnetic resonance structure of monomeric FP in detergent-rich medium (without the rest of the HA2) shows a predominant N-helix/turn/C-helix structure with tight anti-parallel packing of the two helices.^{16,17} In the membrane, the FP shows a mixture of this “closed” structure and a “semiclosed” structure in which the F9 ring is inserted between the two helices.^{18,19} These monomer FP structures may be relevant for the membrane-bound FP in the final hairpin state

of HA2, as EPR spectral line widths of a HA2_{1–127} construct with trimeric SE correlate with monomeric FP domains.²⁰

HA constructs that are truncated in the HA2 TM region result in arrested HA cell/RBC hemifusion with non-expanding pores, which show the importance of a membrane-spanning TM in the final fusion pore expansion step.^{21,22} Fusion is also observed for constructs containing the HA2 ectodomain fused with the TM and endodomain from a different protein.²³ CD spectra of the HA2 TM peptide in detergent and membrane correlate with the expected α -helical structure.²⁴

Earlier studies have shown that large HA2 constructs are hyperthermostable with a T_m of >80 °C. These constructs include HA2_{20–185}≡SE≡SHA2, HA2_{1–185}≡FP+SE≡FHA2, HA2_{20–211}≡SE+TM≡SHA2-TM, and HA2_{1–221}≡full-length HA2.^{25,26} Size-exclusion chromatography (SEC) and cross-linking data often correlate to a large trimer fraction in *N*-lauroylsarcosine (SRC) or *n*-decyl β -D-maltopyranoside (DM) detergent at pH 7.4, with visible aggregation at pH 5.0. The CD θ_{222} values in DM at pH 7.4 correlate with $\sim 60\%$ helicity, which is generally consistent with a trimer-of-hairpins structure for the SE. All four constructs induce fusion of anionic vesicles at pH 5.0, with significant contributions to fusion from the SE and FP. Exogenous addition of constructs like FHA2 or the shorter HA2_{1–127} induces hemifusion and pore formation between “HA0” cells bound to RBC's, where HA0 cells express uncleavable HA's that do not induce fusion.^{27,28}

This study describes structural, biophysical, and functional studies of the G1E and I173E mutants of FHA2 and HA2, with comparison to their WT counterparts. Both mutants result in nearly complete loss of HA cell/RBC fusion and also complete loss of HA0 cell/RBC fusion mediated by exogenously added FHA2.^{10,13,27,28} The N-terminal G1E mutant is in the FP, whereas the I173E mutant is in the SE. For the hairpin structure, I173 is in the exterior strands that bind to the grooves of the interior helical bundle. Some data are consistent with shallower membrane insertion of G1E versus WT FP.²⁹ To the best of our knowledge, no biophysical data for the I173E mutant have been published.

■ MATERIALS AND METHODS

Materials. Some purchased materials were DNA primers (Integrated DNA Technologies, Coralville, IA), *Escherichia coli* strain BL21(DE3) (Novagen, Gibbstown, NJ), Luria-Bertani (LB) medium (Dot Scientific, Burton, MI), isopropyl β -D-thiogalactopyranoside (IPTG) (Goldbio, St. Louis, MO), Cobalt affinity resin (Thermo Scientific, Waltham, MA), *n*-decyl β -D-maltopyranoside (DM) (Anatrace, Maumee, OH), and 1-palmitoyl-2-oleoyl-*sn*-glycero-3-phosphocholine (POPC), 1-palmitoyl-2-oleoyl-*sn*-glycero-3-[phospho-*rac*-(1-glycerol)] (sodium salt) (POPG), 1,2-dioleoyl-3-trimethylammonium propane (DOTAP), *N*-(7-nitro-2,1,3-benzoxadiazol-4-yl) (ammonium salt) dipalmitoylphosphatidylethanolamine (*N*-NBD-DPPE), and *N*-(lissaminerhodamine B sulfonyl) (ammonium salt) dipalmitoylphosphatidylethanolamine (*N*-Rh-DPPE) (Avanti Polar Lipids, Alabaster, AL). Most other materials were purchased from Sigma-Aldrich (St. Louis, MO).

Protein Constructs, Expression, and Purification. The plasmids containing the DNA sequences of full-length HA2_{1–221} and the FHA2≡HA2_{1–185} ectodomain were extracted from previously subcloned *E. coli* cell cultures.²⁶ The G1E and I173E mutants of FHA2 and HA2 were generated by polymerase chain reaction using DNA primers

and confirmed by DNA sequencing (Figures S1 and S2). Each pET24a(+) plasmid was transformed into BL21(DE3) competent cells that were then streaked on an agar plate. After overnight growth in agar, a single colony was transferred to 50 mL of LB medium and grown overnight. All media contained 50 mg/L kanamycin antibiotic, and growth cultures were shaken at 180 rpm and 37 °C. Stock aliquots for future growths were made by mixing 1 mL of culture and 0.5 mL of 50% glycerol and stored at -80 °C. An expression culture was prepared by adding 50 μ L of stock to 50 mL of LB medium, followed by overnight growth, and then addition of 1 L of fresh LB medium and growth until the OD₆₀₀ reached \approx 0.5. Protein expression was induced by addition of 1 mM IPTG and then continued for 5 h at 37 °C. The culture was centrifuged at 9000g and 4 °C for 10 min, and the cell pellet was harvested and stored at -20 °C.

Purifications from cells expressing WT-, G1E-, and I173E-FHA2 were based on earlier work and denoted protocol A.²⁶ Buffers were prepared at 4 °C. Wet cells (5 g) were subjected to four rounds of sonication in 40 mL of buffer A [50 mM sodium phosphate (pH 8.0), 0.5% *N*-lauroylsarcosine (SRC), 300 mM NaCl, and 10 mM imidazole] in an ice bath. Each round lasted for 1 min, with 80% amplitude intervals for 0.8 s followed by 0.2 s off. The lysate was centrifuged at 48000g and 4 °C for 20 min, and subsequent purification was performed at ambient temperature using cold buffers. The lysate supernatant and 1 mL of Co²⁺ affinity resin were stirred for 1 h, and the protein-coated resin was then collected by pouring the suspension through a fritted column. Weakly bound proteins were removed from the resin by washes (four times) with buffer A, with wash volumes of 1 mL (WT-FHA2) or 2 mL (G1E- and I173E-FHA2). Subsequent elutions were performed with buffer B [50 mM sodium phosphate (pH 8.0), 0.5% SRC, 300 mM NaCl, and 250 mM imidazole]. The elutions (4 \times 0.5 mL) were individually characterized by SDS-PAGE, and those with the highest purities and largest quantities of FHA2 were pooled.

Low-yield and low-purity protein was obtained when protocol A was applied to cells expressing WT-HA2, so a new protocol B was developed for HA2 that began with sonication of 5 g of wet cells in 40 mL of phosphate-buffered saline (PBS) [10 mM sodium phosphate and 2 mM potassium phosphate (pH 7.4) with 137 mM NaCl and 3 mM KCl] using the same sonication parameters described above, followed by removal of the supernatant. The remaining pellet was subjected to sonication in fresh PBS and removal of the supernatant, and the new pellet was also subjected to this procedure. The final pellet was then subjected to a purification protocol similar to that used for FHA2-expressing cells, including sonication in buffer A, centrifugation of the suspension, and affinity purification of the supernatant. The eluent was mixed with an equal volume of ice-cold buffer that contained 10 mM Tris (pH 8.0), 0.17% DM, 2 mM EDTA, and 1 M L-arginine, followed by mixing overnight at 4 °C.^{26,30,31}

CD, SEC, Cross-Linking, and Vesicle Fusion. Protein samples for biophysical experiments were prepared by dialysis of the FHA2 purification eluent or HA2 in a buffer with 1 M L-arginine. For CD, SEC, and vesicle fusion, the dialysis buffer contained 10 mM Tris (pH 7.4), and for cross-linking, the buffer contained 20 mM HEPES (pH 7.4). The dialysis buffer also contained either 0.10% SRC or 0.17% DM and, for SEC and vesicle fusion, 150 mM NaCl. Dialysis buffer was replaced each day for the 3 day total dialysis time (5 days for CD

samples). The protein concentration was then adjusted by dilution or by a concentrator.

CD spectra of protein (15 μ M) in buffer with DM were acquired with a CD instrument (Chirascan, Applied Photophysics), in a temperature-controlled cuvette with a 1 mm path length, a 190–260 nm wavelength range, 0.5 nm wavelength increments, and a 1.5 s averaging time per wavelength point. Each displayed spectrum is the difference between the protein with buffer and buffer-only spectra.

SEC was performed with a fast protein liquid chromatography instrument (DuoFlow Pathfinder 20, Bio-Rad), a semipreparative column (Tricorn Superdex 200 Increase 10/300 GL, GE Technologies), a 0.3 mL/min flow rate, and A₂₈₀ detection. The column was equilibrated with an initial run with dialysis buffer without protein. Subsequent SEC was performed with \approx 1 mg/mL loading protein, which corresponds to \approx 0.1 mg/mL running protein.

Cross-linking between lysine ϵ -NH₂ groups was achieved by stirring protein (20 μ M) with bis(sulfosuccinimidyl) suberate (1 mM) for 1 h. The reaction was quenched by addition of Tris-HCl buffer (pH 6.8), with a final Tris concentration of 50 mM, and products were assayed by SDS-PAGE.

Vesicles for fusion studies contained POPC, POPC and POPG (4:1), or POPC and DOTAP (4:1). PC is a common lipid headgroup of the membranes of host cells infected by influenza virus.^{32,33} The PG lipids are included to reflect the negatively charged lipids in the cell membrane. The DOTAP headgroup has a charge of +1 and provides an additional probe of electrostatic effects on fusion. The role of protein charge is probed by comparison of fusion at physiological pH 7.4 and 5.0, where the latter is in the range of 5–6 of influenza fusion with the endosome. The protein charge is approximately -10 at pH 7.4 and +2 at pH 5.0, whereas the lipid charges do not change with pH. Lipids were dissolved in a chloroform/methanol solution [9:1 (v/v)], followed by solvent evaporation with nitrogen gas and vacuum pumping. The resulting lipid films were suspended in 5 mM HEPES and 10 mM MES (pH 7.4 or 5.0), with 0.01% NaN₃. Fluorescently labeled vesicles were similarly prepared, with additional 2 mol % fluorescent lipid (*N*-NBD-DPPE) and 2 mol % quenching lipid (*N*-Rh-DPPE). The lipid suspensions were subjected to 10 freeze/thaw cycles followed by multiple extrusions through a filter with 100 nm diameter pores that produced unilamellar vesicles with a diameter of \sim 200 nm. Labeled and unlabeled vesicles were mixed in a 1:9 ratio with 150 μ M total lipid. HA2-induced fusion between labeled and unlabeled vesicles was detected as an increase in fluorescence due to a larger average distance between fluorescent and quenching lipids. Assay conditions included vesicle stirring at 37 °C, continuous excitation with 467 nm radiation, and gated detection of fluorescence at 530 nm with 1 s time increments. The initial fluorescence of the vesicle solution is denoted F_0 , and addition of HA2 stock marks $t = 0$, with $F(t)$ then measured for \sim 600 s. The stock contained 40 μ M HA2 and 0.17% DM in pH 7.4 buffer with 150 mM NaCl, and the mixed solution had an HA2:lipid mole ratio of 1:300 and 0.002% DM. Subsequent addition of 12 μ L of 20% Triton X-100 detergent solubilized the vesicles and provided F_{\max} . The percent vesicle fusion is calculated as $\{[F(t) - F_0]/F_{\max} - F_0\} \times 100$. There is the typical \pm 1% variation in long-time fusion extent between assay replicates, and there is negligible fusion after addition of an aliquot of stock buffer without protein. Although our conversion of fluorescence increases to percent vesicle fusion

is standard practice, the calculated fusion is not a quantitative measure of percent fused vesicles. The fluorescence varies as $[1 + (R_0/R_{FQ})^6]^{-1}$, where R_0 and R_{FQ} are the Forster and average fluorophore–quencher distances, respectively, so fluorescence changes and percent lipid mixing are sensitive to the initial fluorophore and quencher concentrations. The most meaningful fusion comparisons are between different proteins with the same vesicle stock and between different vesicle compositions using the same protein stocks.

RESULTS

Protein Preparation and Folding. Figure 2 displays SDS–PAGE of the purification eluents. The purified yields of WT-,

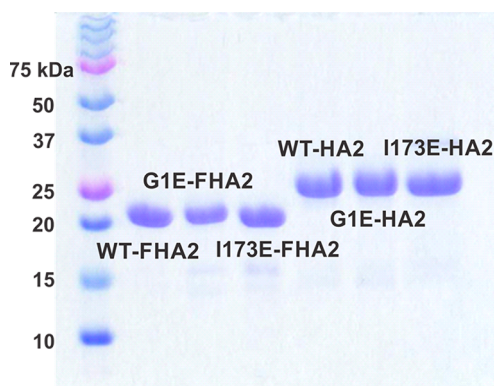


Figure 2. SDS–PAGE of the purification eluents. $MW_{FHA2} = 22.4$ kDa, and $MW_{HA2} = 26.7$ kDa.

G1E-, and I173E-FHA2 are ~ 10 , 5, and 3 mg/L of culture, respectively, whereas the yields of the corresponding HA2 variants are ~ 2 , 1, and 0.7 mg/L of culture, respectively. High-purity FHA2 proteins were obtained by protocol A with affinity chromatography of the supernatant of the SRC-solubilized cell lysate. The proteins were well-folded after dialysis into buffer with DM, as evidenced by prominent minima in the CD spectra at 208 and 222 nm, which are characteristic of the expected predominant α -helical structure. Quantitative analysis of the $|\theta_{222}|$ values is presented in the CD results. Application of protocol A to cells that expressed HA2 resulted in low-yield and low-purity HA2. Reasonable yields of high-purity HA2 proteins were obtained by protocol B for which there was an initial step of removal of PBS soluble and suspendable material, followed by solubilization of the remaining cell pellet with sonication in buffer with SRC, and then affinity purification. The HA2 product was pure but not well-folded, based on a small $|\theta_{222}|$ value of the CD spectrum obtained after direct dialysis into buffer with DM. Well-folded HA2 was obtained if there was intermediate dialysis into buffer with DM and 1 M L-arginine, followed by dialysis into buffer with DM and no L-arginine. These data support folded HA2 as the lowest-free energy state in buffer with DM. The L-arginine may break up partially misfolded HA2 aggregates.

We describe a model that explains the underlying bases of the different protocols to obtain pure and well-folded FHA2 and HA2, as well as the different yields. We first consider the protocol B initial sonications in PBS, with discarding of the PBS supernatants obtained after centrifugation at 48000g. The HA2 content of the initial PBS supernatant was investigated by centrifugation at 22000g and then subjecting the pellet to protocol A. The resulting eluent contained very pure HA2 that

was well-folded, as judged by the CD spectrum after direct dialysis into buffer with DM. However, the HA2 yield from this “22000g pellet” was much lower than the yield of partially folded HA2 from the “48000g pellet” of protocol B. We interpret our results as supporting FHA2/HA2 locations both in the bacterial membrane and in inclusion bodies, with well-folded and partially folded molecular structures, respectively. The protocol A supernatant from SRC sonication of cells expressing FHA2 contains mostly membrane-located FHA2, whereas the protocol B supernatant from SRC sonication of cells expressing HA2 contains mostly inclusion body HA2. The discarded supernatants from the protocol B initial sonications in PBS contain a small quantity of membrane-suspended and well-folded HA2. Overall, these data evidence that SRC is an effective detergent for both membrane and inclusion body FHA2/HA2 and solubilizes more rapidly the folded membrane fractions of these proteins. The latter idea is consistent with the results of protocol A for FHA2, including folded FHA2 and a substantial pellet that is not purified and contains predominantly partially folded inclusion body FHA2. The latter point is supported by previous purification of FHA2 from this pellet, with a yield of ~ 10 mg of FHA2/L of culture that is comparable to the yield of protocol A.³¹ This inclusion body FHA2 was well-folded only when there was intermediate dialysis into buffer with 1 M L-arginine and DM.

We estimate a >10 -fold higher level of expression of FHA2 than of HA2 based on ~ 5 -fold greater purified yields of WT-, G1E-, and I173E-FHA2 via protocol A versus their HA2 counterparts via protocol B, ~ 2 -fold greater yields of purified FHA2 from complete solubilization of the cell pellet versus the protocol A partial solubilization, and detection of FHA2 but not HA2 in the washes of the Co^{2+} resin with bound protein. The lower purified yields of G1E and I173E versus WT proteins probably have some contribution from different expression levels, as the ratio of purified yields for FHA2 to HA2 is ~ 5 for the WT, G1E, and I173E variants. All of the reported yields are from sonications with 40 mL of buffer. For protocol B, there was complete solubilization in 40 mL of buffer with SRC for the pellet from cells expressing WT-HA2, whereas 50 mL was required for the pellets from cells expressing G1E- or I173E-HA2. Use of 50 versus 40 mL resulted in ~ 0.3 mg/L greater purified yields of G1E- and I173E-HA2.

Size-Exclusion Chromatography and Cross-Linking.

Figure 3 displays (left) SEC before cross-linking and (right) SDS–PAGE after cross-linking. Data were obtained in (A) SRC and (B) DM detergents. Data for replicate samples are presented in Figure S3. Individual SEC elution peaks and cross-linking bands are assigned to the monomer, dimer, trimer, and aggregate. Data for WT proteins are similar to previous results.²⁶ For all proteins in SRC and HA2 proteins in DM, there is a large SEC peak at ~ 250 kDa that is assigned to a trimer with ~ 75 kDa protein and ~ 175 kDa detergent contributions. This SEC assignment is consistent with earlier observations, including an $\sim 1:120$ protein:detergent mole ratio for a HA2 fusion protein trimer and dominant trimer for the HA2 soluble ectodomain in aqueous solution.^{25,30} Several of the SEC traces exhibit a peak at ~ 40 kDa that is assigned to a monomer with ~ 25 kDa protein and ~ 15 kDa detergent contributions. This is a major peak for the I173E mutants in DM and a minor peak in other traces. Some traces also exhibit a minor peak at ~ 150 kDa that is assigned to the dimer with ~ 50 kDa protein and ~ 100 kDa detergent contributions. Both

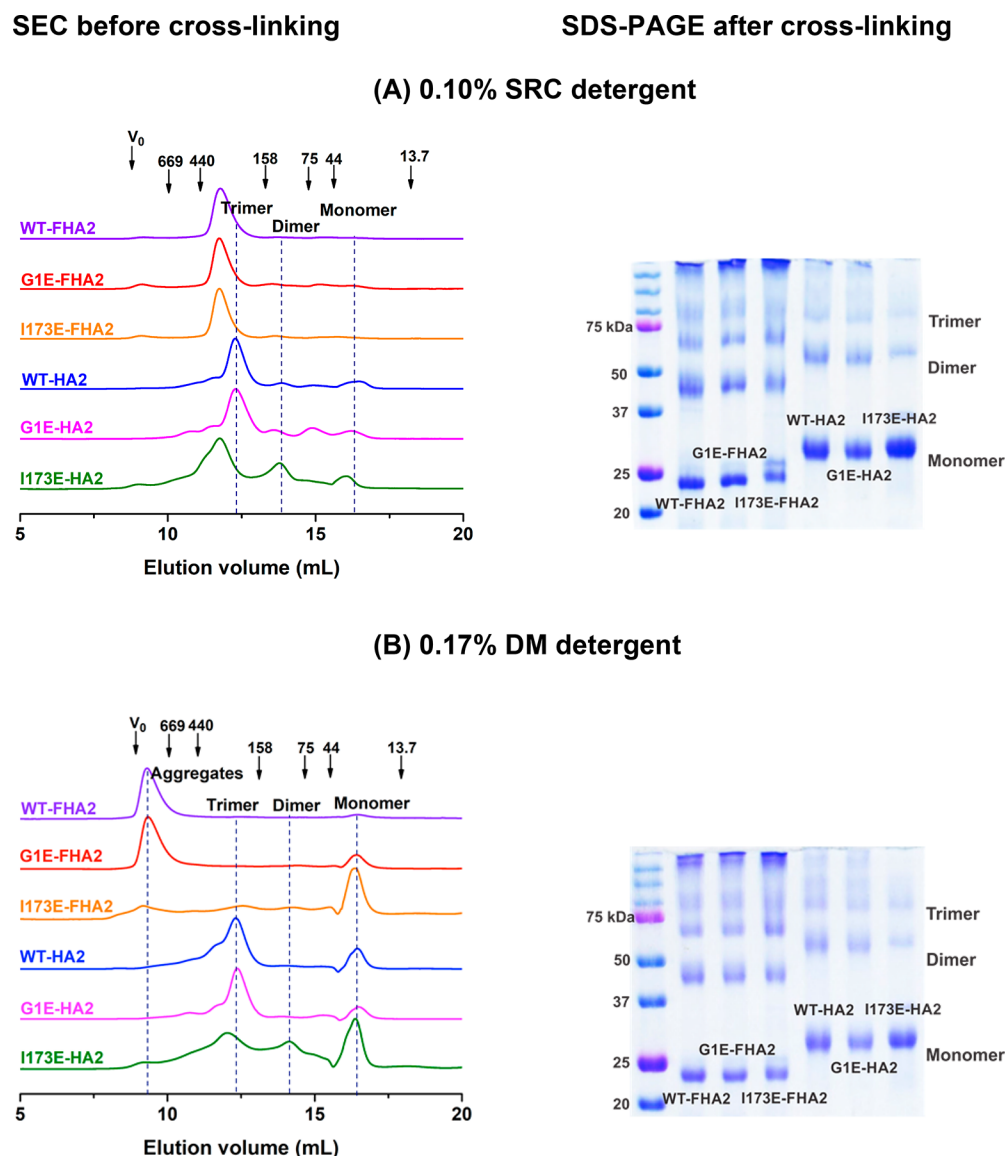


Figure 3. SEC traces prior to cross-linking (left) and SDS-PAGE after cross-linking (right) and in (A) SRC and (B) DM detergents. SEC parameters include 1 mg/mL loading protein concentration, ≈ 0.1 mg/mL running protein concentration, and A_{280} detection. Arrows mark the elution volumes of the void (V_0) and MW standards in kilodaltons. Cross-linking conditions include 0.5 mg/mL protein, a 50-fold molar excess of bis(sulfosuccinimidyl) suberate cross-linking agent, and 1 h time. The gels were made using 12% acrylamide. See Figure S3 for data on replicate samples.

WT- and G1E-FHA2 proteins in DM have a dominant peak in the void volume corresponding to oligomers/aggregates with MW's of >1 MDa.

After cross-linking, the monomer is the most intense band for all constructs in both detergents, followed by the dimer and trimer. Higher-MW bands are weaker, except for those of FHA2 constructs, which exhibit a band for large aggregates that does not migrate in the gel. The cross-linking data are generally consistent with the monomer, dimer, and trimer peaks observed in SEC, with the caveat that the cross-linking reaction is not complete so that the band intensities do not reflect populations.

Circular Dichroism. Figure 4 presents CD spectra of the six constructs in DM at pH 7.4 and ambient temperature. These data were taken on the same day using the same CD spectrometer. Data for replicate samples are presented in Figure S4 and typically exhibit $\pm 5\%$ variation in θ_{222} values

among replicates. All constructs exhibit spectra characteristic of α -helical structure, with minima at 208 and 222 nm. Table 1 reports average helicities calculated from θ_{222} values, with higher helicity for FHA2 than for HA2 and for WT and G1E than for I173E. The similar helicities of G1E and WT proteins are consistent with helical FP structure for G1E, whereas the reduced helicity of I173E proteins supports some disruption of the SE structure in this mutant. There is not NaCl in the sample buffers for the CD spectra shown in Figure 4, but Figure S5 shows that for I173E-FHA2, similar spectra are obtained in the absence and presence of 150 mM NaCl. Figure S5 also presents spectra with 1, 5, 10, and 20 μ M I173E-FHA2, and all the θ_{222} values correlate to a significant fraction of α -helical structure.

Figure 5 displays CD spectra obtained between 25 and 90 $^{\circ}$ C in 5 $^{\circ}$ C increments, and Figure 6 displays plots of θ_{222} versus temperature. All spectra for a particular construct were

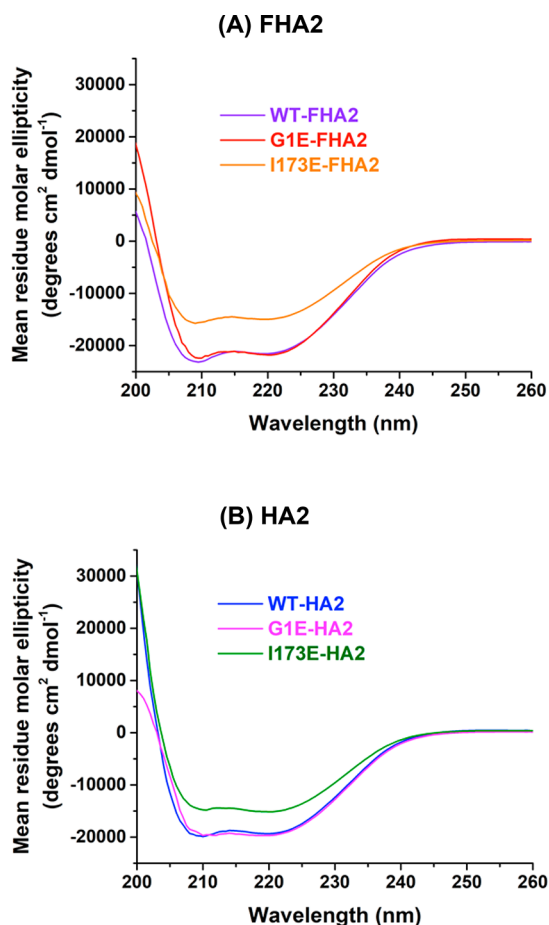


Figure 4. CD spectra of the (A) FHA2 and (B) HA2 proteins at ambient temperature. Samples contained 15 μ M protein in 10 mM Tris buffer (pH 7.4) with 0.1% DM. See Figure S4 for spectra of replicate samples.

acquired on the same day. Thermostabilities of constructs are qualitatively ordered as follows: WT-HA2 > WT-FHA2 > G1E-HA2 and I173E-HA2 > G1E-FHA2 > I173E-FHA2. The θ_{222} value at each temperature is used to calculate the fraction folded protein via the equation $f_{\text{folded}} = |\theta_{222} - \theta_{\text{unfolded}}| / |\theta_{\text{folded}} - \theta_{\text{unfolded}}|$ and then $f_{\text{unfolded}} = 1 - f_{\text{folded}}$. The model equilibrium is folded trimer \leftrightarrow 3 unfolded monomers, so that $K_{\text{eq}} = (f_{\text{unfolded}})^3 / (1 - f_{\text{unfolded}}) / 3$. The unfolded state is likely a monomer rather than trimer because (1) the favorable hydrophobic effect of the trimer is achieved with folded monomer units but not unfolded units and (2) the translational entropy is greater for three independent monomers than for a trimer. The van't Hoff analysis of $\ln K_{\text{eq}}$ versus $1/T$ is linearly fitted, and the best-fit slope and $\ln K_{\text{eq}}$ intercept are used to calculate $\Delta H_m = -R \times \text{slope}$, $\Delta S_m = R \times \ln K_{\text{eq}}$ intercept, and $T_m = \Delta H_m / \Delta S_m$ that corresponds to $\ln K_{\text{eq}} = 0$ (Table 1). The T_m values for G1E-FHA2 and I173E-FHA2 are near the middle of the 25–90 °C experimental temperature range, and the $\ln K_{\text{eq}}$ versus $1/T$ plots are reasonably linear over the whole range (Figure 7). The T_m values are higher for the other proteins, and the $\ln K_{\text{eq}}$ versus $1/T$ plots are linear for only the temperature range around T_m over which $\ln K_{\text{eq}}$ changes sign and exhibits significant changes in magnitude (Figure S6). The numbers in parentheses in Table 1 are the fitting-associated uncertainties of the parameter values. There are also uncertainties in the θ_{folded} and θ_{unfolded}

Table 1. Analysis of CD Spectra

construct	average percent helicity ^a	T_m ^{b,c} (°C)	ΔH_m (kcal/mol)	ΔS_m (cal mol ⁻¹ K ⁻¹)
WT-FHA2	64	86.8(0.2)	186(11)	517(29)
G1E-FHA2	65	55.2(1.3)	49.1(1.0)	149.6(3.0)
I173E-FHA2	44	45.4(2.7)	30.1(1.3)	94.4(3.8)
WT-HA2	58	90.7(1.2)	126(36)	345(99)
G1E-HA2	58	75.0(2.4)	43.6(3.6)	125(11)
I173E-HA2	45	79.2(1.2)	165(17)	469(48)

^aCalculated using the θ_{222} of ambient-temperature CD spectra, with 100% helicity taken as $\theta_{222} = -33000$ deg cm² dmol⁻¹. ^bThe T_m , ΔH_m , and ΔS_m parameters are calculated using van't Hoff analysis of $\ln K_{\text{eq}}$ vs $1/T$, where $K_{\text{eq}} = (f_{\text{unfolded}})^3 / (1 - f_{\text{unfolded}}) / 3$, $f_{\text{folded}} = |\theta_{222} - \theta_{\text{unfolded}}| / |\theta_{\text{folded}} - \theta_{\text{unfolded}}|$, $f_{\text{unfolded}} = 1 - f_{\text{folded}}$, and θ_{unfolded} values are based on extrapolations from $\theta_{25^\circ\text{C}}$ and $\theta_{90^\circ\text{C}}$, respectively. Fitting is done over the temperature range for which $\ln K_{\text{eq}}$ changes sign and exhibits significant changes in magnitude, and over which $\ln K_{\text{eq}}$ vs $1/T$ is reasonably linear. $\Delta H_m = -R \times \text{slope}$; $\Delta S_m = R \times \ln K_{\text{eq}}$ intercept, and $T_m = \Delta H_m / \Delta S_m$. Specific θ_{folded} and θ_{unfolded} values in units of deg cm² dmol⁻¹ and fitting temperature ranges in units of °C are as follows: WT-FHA2, -18000, -2000, and 80–90; G1E-FHA2, -17000, -1500, and 25–85; I173E-FHA2, -21000, -2700, and 25–90; WT-HA2, -19000, -2000, and 80–90; G1E-HA2, -19500, -500, and 55–90; I173E-HA2, -15000, -900, and 70–90, respectively. ^cThe numbers in parentheses are fitting-associated uncertainties. The uncertainties in the ΔH_m and ΔS_m parameters are based on statistically reasonable variations in the sum of residuals $\sum_j (\ln K_j^{\text{exp}} - \ln K_j^{\text{calc}})^2$, where exp indicates experimental, calc indicates calculated, and j is the data index. Variations in ΔH_m and ΔS_m are highly correlated with one another. The uncertainty in $T_m \equiv \delta_{T_m}$ was calculated using the variation in $1/T \equiv \delta_{1/T}$ associated with the average residual $\equiv \delta_{\ln K}$. The relationships $\delta_{1/T} = \delta_{\ln K} / (\Delta H_m / R)$ and $\delta_{1/T} / (1/T_m) = \delta_{T_m} / T_m$ were the basis for the calculated $\delta_{T_m} = \delta_{1/T} \times T_m^2$.

values that are chosen on the basis of extrapolations from the respective $\theta_{25^\circ\text{C}}$ and $\theta_{90^\circ\text{C}}$. These θ uncertainties result in uncertainties in the calculated f_{unfolded} , $\ln K_{\text{eq}}$, and fitted parameter values. Changes in θ_{folded} and θ_{unfolded} typically lead to <2 °C changes in T_m .

Vesicle Fusion. Figure 8A displays traces of HA2-induced PC vesicle fusion versus time at pH 5.0, and Figure 8B displays long-time fusion extents for PC, PC/PG (4:1), and PC/DOTAP (4:1) vesicles at pH 5.0 and 7.4. Figure S7 displays fusion extents from replicate assays with different protein and vesicle preparations. The trends for each protein are typically similar among the figures for pH 5.0 and 7.4 and for PC/PG and PC/DOTAP vesicles. Influenza virus fuses with the late endosome at pH <6. At pH 5.0 and 7.4, PC has a neutral zwitterionic headgroup, and PG and DOTAP carry charges of -1 and +1, respectively. The membranes of host cells of influenza contain ~25 mol % PC and ~15 mol % anionic lipid, including PG, and there are widely varying lipid compositions of the chromatographic fractions of endosomal membranes.^{26,32–35} The influenza virus also fuses with vesicles with a variety of lipid compositions.³⁶ Although there are not physiological positively charged lipids, PC/DOTAP vesicles are studied to probe the effect of the sign of the lipid charge on fusion. The HA2:lipid mole ratio of 1:300 of the assay is smaller than the ~1:50 ratio of the virus.^{37,38} HA-mediated fusion includes lipid mixing as well as pore formation, leakage,

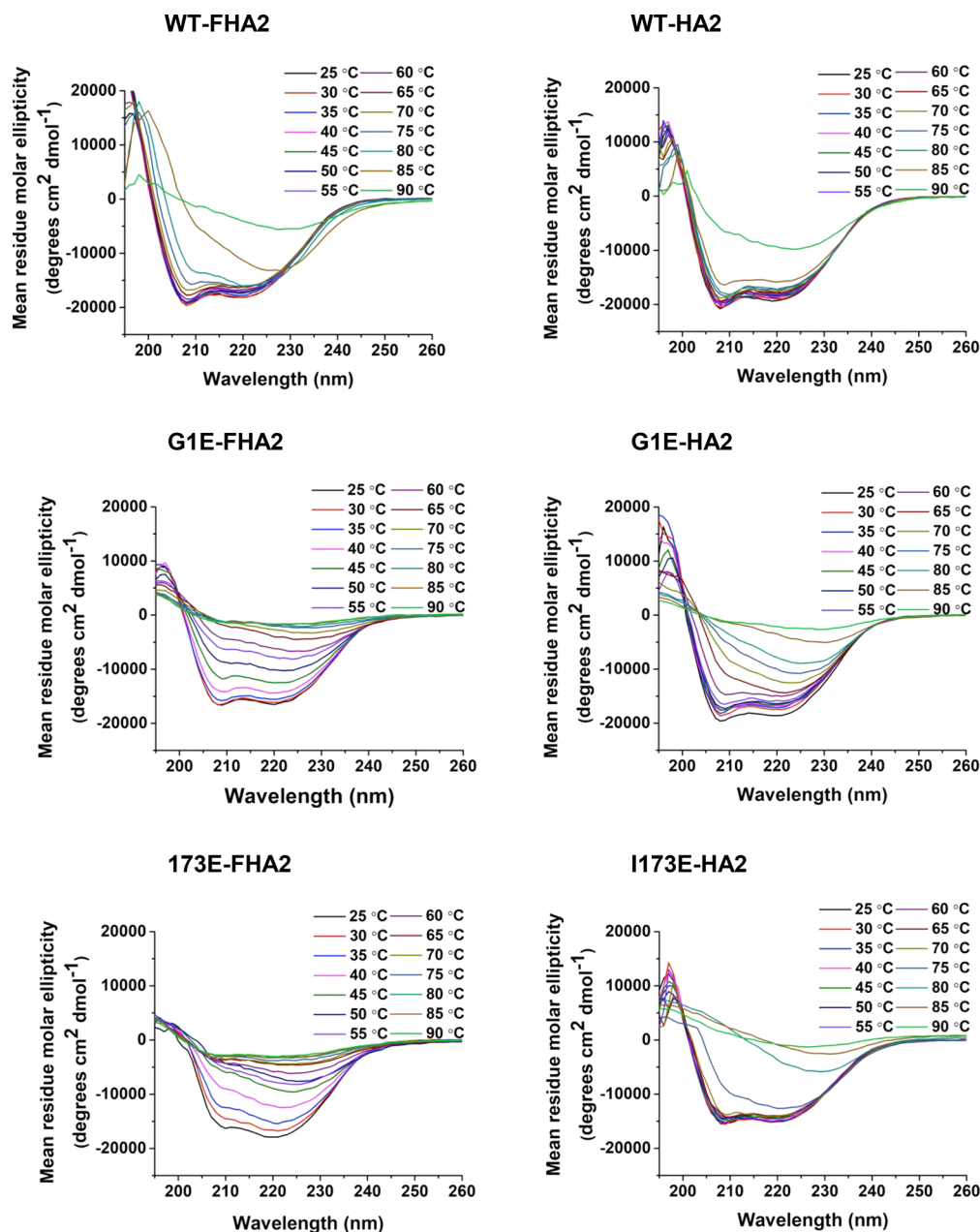


Figure 5. Temperature-series CD spectra. Protein and buffer conditions are the same as in Figure 4.

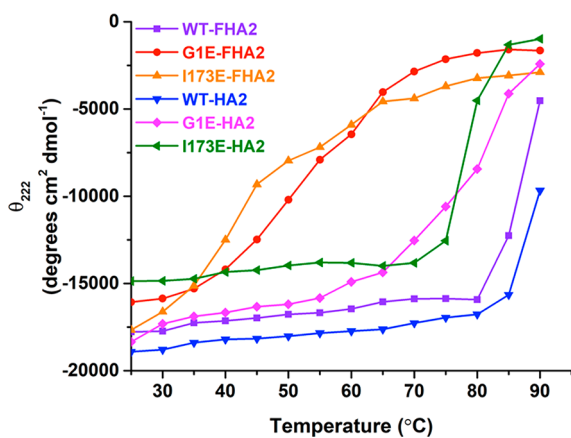


Figure 6. Plots of θ_{222} vs temperature.

and content mixing.^{12,13,36} Protein-mediated vesicle fusion exhibits faster leakage than content mixing, and in the study presented here, vesicle fusion is assayed by lipid mixing, which is a common feature with HA fusion.^{39,40}

Figure 8A shows much more extensive PC vesicle fusion at pH 5.0 for WT-HA2's than for mutant HA2's, with similar reduced levels of fusion for both G1E and I173E. Figure 8B shows that the level of PC fusion is reduced at pH 7.4 but still higher for WT versus the mutant. At pH 5.0, there is lower level of fusion of PC/PG than of PC vesicles, while at pH 7.4, there is similar reduced level of fusion for both vesicle types. At pH 5.0, the calculated WT-HA2 charge is +3, so the higher level of fusion of PC versus PC/PG shows that attractive HA2/vesicle electrostatic energy is not required for fusion catalysis. This conclusion is similarly supported by significant fusion of PC/DOTAP vesicles at both pH's, even though there are respective repulsive versus attractive HA2/vesicle electrostatic

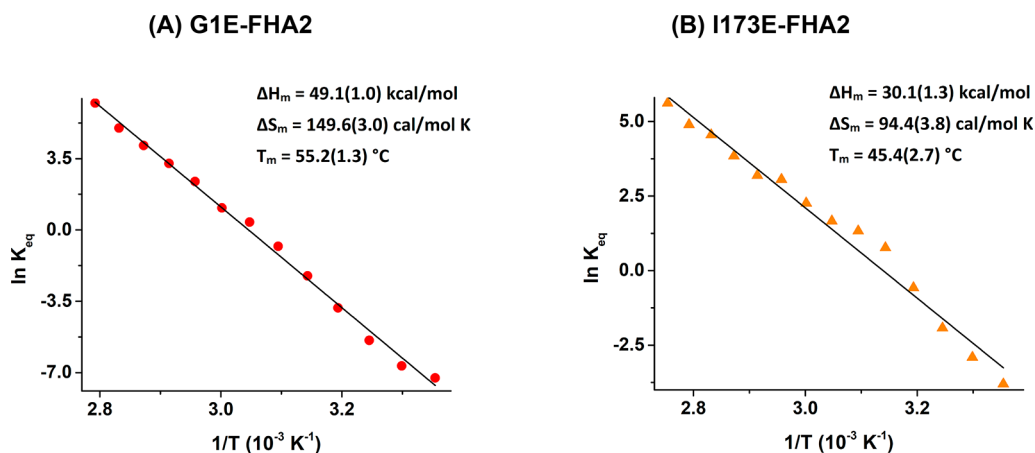


Figure 7. van't Hoff plots of the unfolding $\ln K_{eq}$ vs $1/T$ of the (A) G1E-FHA2 and (B) I173E-FHA2 proteins based on θ_{222} data for the temperature range around T_m . Best-fit parameters are given with uncertainties in parentheses.

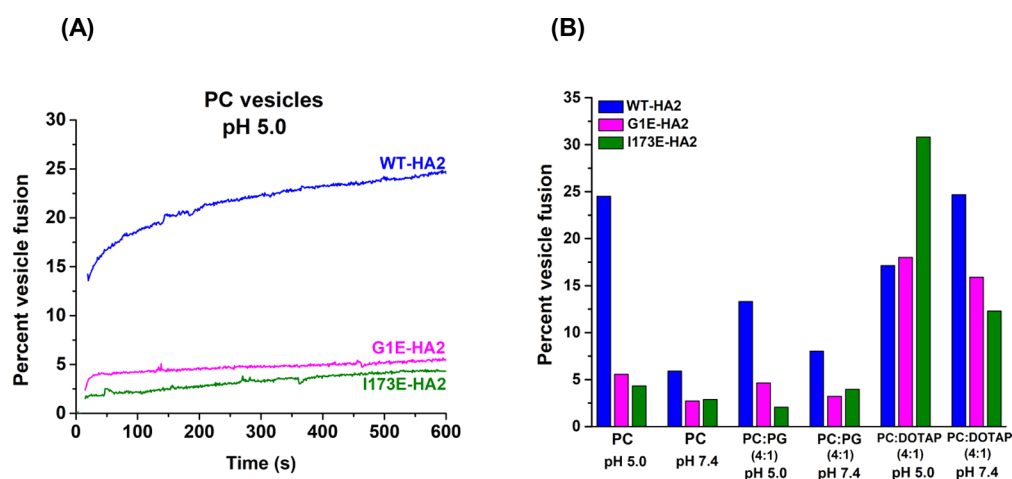


Figure 8. HA2-induced vesicle fusion with a 1:300 protein:lipid ratio. (A) Time courses of POPC vesicle fusion at pH 5.0. (B) Percent vesicle fusion at 600 s after addition of protein for different lipid compositions and pH's. Each bar represents the average of three replicates. There is typically a $\pm 1\%$ variation in percent vesicle fusion among the replicates. See [Figure S7](#) for data using different preparations of proteins and vesicles.

energies at pH 5.0 vs pH 7.4. Detailed interpretations of the fusion extents are presented in the [Discussion](#).

DISCUSSION

This study describes a structural and functional comparison between full-length WT-HA2 and the truncated construct lacking the TM, FHA2, and the G1E and I173E point mutants that are known to inhibit HA-mediated fusion. Significant findings of the present study include (1) a predominant trimer fraction in SRC detergent at pH 7.4 for all protein constructs versus mixtures of the trimer, monomer, and oligomers/aggregates in DM detergent, (2) similar helicities of WT and G1E proteins versus the reduced helicity of I173E proteins, (3) hyper-thermostable WT-FHA2 and HA2 and less stable FHA2 and HA2 mutants with respective reductions in T_m of ~ 40 and ~ 15 °C, and (4) efficient HA2-induced vesicle fusion of neutral and anionic vesicles at pH 5.0 for WT-HA2 versus a reduced level of fusion with mutants.

Models of Protein Structure and Stability. The CD spectra and analyses of [Figure 4](#) and [Table 1](#) support a 65% average helicity for WT- and G1E-FHA2 and a 58% average helicity for WT- and G1E-HA2. The proteins are well-folded, based on reasonable agreements between these average helicities and the fractions of α -helical residues calculated for

a model in which the only α -helical residues are those in high-resolution structures of the FP in detergent and the SE in aqueous solution, and in the TM [residues 2–12, 14–22, 38–105, 110–128, 146–153, and 186–210 ([Figure 1B](#))].^{8,16} The calculated helical fractions from this model are 115/193 residues for FHA2 and 140/235 residues for HA2. The helicities of WT-FHA2 and HA2 determined in this study are similar to the helicities reported in some earlier studies.^{26,31,41} However, the 65% helicity for WT- and G1E-FHA2 in this study is higher than the helicities of ~ 25 and $\sim 35\%$, respectively, from a 2011 study.²⁸ The origin of this discrepancy is not known, but we note that our high and their low helicities correlate with the presence and absence, respectively, of detergent in the samples. Our study also shows that the I173E mutants exhibit only 45% helicities, and a model explaining this reduced helicity is presented below.

The hyperthermostabilities of WT-FHA2 and HA2 are evidenced by the CD spectra and θ_{222} versus T plots ([Figures 5](#) and [6](#)) and the accompanying van't Hoff analyses for determining T_m values ([Table 1](#)). The T_m of ≈ 90 °C for FHA2 and HA2 and the T_m values of ≈ 80 °C for HA2_{20–185} (SE) and >85 °C for HA2_{20–211} (SE+TM) support a major contribution to stability by the SE, with smaller contributions from the FP and TM, where the latter two HA2 domains are

the only ones that are deeply inserted in the fused membrane.^{25,26,42} The hairpin structure of the SE in the final HA2 state allows for proximity between residues 1–37 and 177–210 that could be the basis of the higher T_m of full-length HA2 versus its truncated constructs. In previous papers, this possibility has been imagined as a bundle complex between the three FP's (e.g., HA2_{1–23}) and three TM's (e.g., HA2_{187–209}).^{2,11}

The I173E mutation significantly destabilizes the SE of FHA2 as evidenced by loss of 30% of the overall helicity and the reduction of T_m by 40 °C (Table 1). There is smaller but still significant SE destabilization for I173E-HA2 versus WT-HA2. The WT SE structure in Figure 1B has C-terminal strands in the external grooves of the N-helix bundle, with the I173 side chain inserted in a hydrophobic pocket of the bundle. Figure 9 displays a structural model for the I173E SE in which

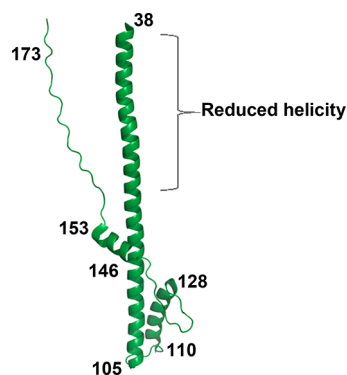


Figure 9. Structural model for a monomer unit of the SE of mutant HA2's. There is partial dissociation of the C-terminal strand and partial unfolding of the N-terminal helix.

there is dissociation of the strands from the bundle, with accompanying destabilization and loss of helicity near the bundle terminus. Strand dissociation is due in part to the more favorable Born energy of the charged Glu side chain in the high-dielectric aqueous environment versus the low-dielectric protein interior. This I173E model is supported by data for shorter HA2 constructs with C-terminal truncation. The HA2_{38–89} peptide forms a trimer of parallel helices at lower temperatures and unfolded monomers at higher temperatures, and its T_m of 51 °C is comparable to the T_m of I173E-FHA2.⁴³ Ambient-temperature CD spectra of HA2_{1–127} correlate with 50% helicity, which is much lower than the value of 85% (106/127 residues) calculated using helical regions of the FP and SE structures.⁴⁴

G1E- and WT-FHA2 both exhibit 65% ambient-temperature helicity, but the T_m for G1E-FHA2 is reduced by 32 °C versus that of WT-FHA2, which indicates significant destabilization of the SE by the G1E mutation. There is less but still significant destabilization of G1E-HA2 versus WT-HA2. Destabilization of the SE is surprising because the G1E mutation is more than 35 residues from the SE structure. We propose that the SE destabilization for G1E is similar to that for I173E and is a result of loss of binding of C-terminal strands with the N-terminal helical bundle (Figure 9). This loss is due to competition with the G1E FP's for binding to the strands. Binding is not expected for the WT-FP that adopts a tight helical hairpin structure that is stabilized by the favorable G1-NH₃⁺/(14–22) helix–dipole interaction (Figure 1B).⁴⁵ This interaction may be disrupted for zwitterionic E1, with

consequent separation of the two FP helices that can then bind with the SE strands.

G1E-FHA2, G1E-HA2, and I173E-FHA2 have ΔH_m values of 49, 44, and 30 kcal/mol, respectively, that are determined from van't Hoff analyses over broad temperature ranges for which there are clear changes from mostly folded to mostly unfolded protein (Figure 7, Figure S6, and Table 1). There are likely similar unfolded monomer states for all of the proteins, so the ΔH_m values likely reflect more favorable enthalpies for folded G1E-FHA2 and HA2 versus I173E-FHA2. This interpretation is consistent with the previously described direct I173E destabilization of binding between the C-terminal strands and the N-terminal helical bundle of the SE versus less direct G1E destabilization of the SE by weakening FP interhelical interactions, with consequent competition by the FP for binding to the strands. There are less accurate ΔH_m values for WT-FHA2, HA2, and I173E-HA2, because these values are determined from van't Hoff analyses from limited temperature ranges, and unfolding is sometimes incomplete at the highest temperature. The ΔH_m values are larger for WT-FHA2 than for G1E- and I173E-FHA2 and WT-HA2 than for G1E-HA2, which is evidence of more favorable enthalpies of the WT proteins. The WT ΔH_m values are similar to those of papain and trypsin, which have masses similar to those of the monomer HA2 constructs.⁴⁶ The ΔS_m and ΔH_m values are correlated in Table 1, as expected from the relationship $\Delta S_m = \Delta H_m/T_m$.

Monomers and Trimers. The SEC data for all constructs in SRC show predominant trimers, with minor populations of monomers and dimers (Figure 3A and Figure S3). The relative populations of different species are more varied between the constructs in DM, and the monomer fractions are generally higher, particularly for I173E-FHA2 and HA2 (Figure 3B and Figure S3). SEC was performed with ≈ 4 μ M protein and 150 mM NaCl, and CD spectra of I173E-FHA2 evidence well-folded protein for these conditions and also for different protein concentrations without NaCl (Figure 4 and Figure S5). The greater monomer fraction of I173E versus WT proteins is correlated with the lower stability of the I173E trimer. To the best of our knowledge, folded monomer HA2 has not been previously reported, but there are reports of the folded monomer HA1+HA2 ectodomain, including complexes with antibodies, and folded monomer gp41.^{47–57} Interestingly, both HA2 and HIV gp41 SE constructs can form folded hyperthermostable monomers and trimers, with similar structures for the monomers and monomer subunits of the trimers. The monomer fraction is correlated with interprotein electrostatic repulsion, as evidenced by larger monomer fractions for HA2 constructs at neutral pH (charge ≈ -10) and for gp41 constructs at low pH (charge $\approx +10$). There are larger populations of trimer and larger oligomers for HA2 at low pH and gp41 at neutral pH, with charges of approximately +2 and –2, respectively. Another similarity between HA2 and gp41 is predominant trimers in anionic detergents, SRC and SDS, respectively, and larger monomer fractions in neutral detergents, DM and DPC, respectively. We hypothesize that the protein trimer may carry <3 times the monomer charge because of protonation of the Asp and Glu side chains in the trimer interior. The trimer may therefore be favored in an anionic detergent because the electrostatic repulsion between the trimer and micelle is weaker than between three monomers and micelles.

Although the SEC data for I173E-FHA2 in DM show predominant monomers, the cross-linking data are consistent with a significant fraction of trimers. This difference may be due to the presence (SEC) versus absence (cross-linking) of NaCl, as other proteins also exhibit smaller oligomer and greater monomer fractions with an increased NaCl concentration.^{58,59} This behavior is sometimes attributed to disruption of salt bridges between monomer units of the oligomer. The HA1+HA2 ectodomains of influenza strains A/Korea/01/2009 (KR01), A/California/04/2009 (CA04), and A/Darwin/2001/2009 (DA01) are monomers in a pH 8.0 solution with 200 mM NaCl, but only the latter two are trimers in their crystal structures; on the other hand, KR01 shows a V-shaped arrangement of two monomers connecting through the HA1 globular head domains.^{49,54} The monomer structure is similar in all three strains. The sequence of KR01 differs at only three residues from those of CA04 and DA01, and the crystallization conditions differ only in 100 mM NaCl for KR01 versus no NaCl for the strains that adopt trimer structures. The presence and absence of NaCl may therefore favor folded monomer and folded trimer HA2, respectively.

Correlations between WT-HA2 Fusion and Electrostatic Energies. Figure 8B displays comparative vesicle fusion extents for WT and mutant HA2's, pH 5.0 versus pH 7.4, and vesicle compositions of zwitterionic PC lipids versus mixtures of PC and anionic PG lipids, or PC and cationic DOTAP lipids. We first focus on WT-HA2 fusion under different conditions and discuss how differences in fusion extents correlate with electrostatic energies. The charge of WT-HA2, excluding the tag, is approximately +3 at pH 5.0 and approximately -9 at pH 7.4, whereas the lipid charges are pH-invariant and are 0 for PC, -1 for PG, and +1 for DOTAP. A higher level of PC fusion at pH 5.0 than at pH 7.4 correlates with weaker intertrimer electrostatic repulsion at pH 5.0 than at pH 7.4. This also correlates with visible aggregation of the HA2 constructs at pH 5.0 that may contribute to fusion via increased local membrane concentrations and perturbations of the FP and perhaps TM.²⁶ These effects are also evidenced by higher levels of PC/PG fusion at pH 5.0 than at pH 7.4, with an additional contribution from attractive versus repulsive HA2/vesicle electrostatic energies. This latter effect is also evident from higher levels of PC/DOTAP fusion at pH 7.4 than at pH 5.0 and corresponding attractive versus repulsive HA2/vesicle electrostatic energies. This energy contribution is also manifested by a higher level of PC/DOTAP fusion at pH 7.4 versus the level of PC/PG fusion at pH 5.0 and the corresponding stronger attraction between the -9 charge HA2 and DOTAP versus the +3 charge HA2 and PG. Similarly, a higher level of PC/DOTAP fusion at pH 5.0 than of PC/PG fusion at pH 7.4 correlates with weaker HA2/DOTAP versus stronger HA2/PG electrostatic repulsion. Vesicle/vesicle electrostatics are manifested by higher levels of fusion for PC versus PC/PG at pH 5.0 and the corresponding neutral versus repulsive intervesicle electrostatic energies. In addition, higher levels of PC/DOTAP fusion at pH 5.0 versus PC fusion at pH 7.4 correlate with the previously described fusion contribution of HA2 aggregation at pH 5.0.

Reduced Levels of Fusion with Mutants. G1E- or I173E-HA cells do not fuse with RBC's (i.e., negligible hemifusion and pore formation), with very similar losses of function of cell/RBC fusion induced by exogenous FHA2 with either of these mutations.^{10,13,28} There are qualitatively similar but less dramatic effects of these mutants on HA2-induced PC

and PC/PG vesicle fusion (Figure 8). The ~4-fold reduction in the level of fusion for G1E-HA2 versus WT-HA2 with PC vesicles matches well with the reduction previously observed for G1E-FHA2 versus WT-FHA2 with PC/cholesterol vesicles.²⁸ Some mutant HA2-induced vesicle fusion versus no mutant HA-cell/RBC fusion is ascribed to the ~10-fold higher density of HA2 trimers in vesicles than of HA trimers in the cell.^{37,38} The importance of HA density for fusion is supported by the correlation between comparable fusion of G1S and WT virions with vesicles versus reduced G1S relative to WT-HA cell/RBC fusion, and the ~50-fold higher density of HA trimers in the virion relative to HA trimers in the cell.⁶⁰

For PC/DOTAP vesicles at pH 7.4, there is reduced level of fusion of mutant HA2 versus WT-HA2, which is qualitatively similar to the PC and PC/PG results. The opposite trend is observed for PC/DOTAP at pH 5.0, with respective comparable and higher fusion extents of G1E- and I173E-versus WT-HA2. This trend correlates with mutant HA2 and WT-HA2 total charges of +2 and +3, respectively, and corresponding weaker mutant versus WT-HA2/DOTAP electrostatic repulsion.

We focus on PC and PC/PG vesicle fusion at pH 5.0 because these lipid compositions and this pH reflect some of the conditions of HA-mediated virus/endosome fusion. Relative to WT-HA2, G1E- and I173E-HA2 exhibit similar reductions in the level of fusion that correlate with their lower SE hairpin stabilities. A more open hairpin could reduce the level of fusion via the larger separation of vesicles bound to the terminal FP and TM segments. In addition, the mutant HA2's may have less FP/membrane interaction because of the stronger FP interaction with the dissociated C-terminal SE region (Figure 9). A reduced level of I173E-HA2 fusion may also be associated with its higher monomer:trimer ratio (Figure 3 and Figure S3). Relative to the trimer, the monomer protein has lower local concentrations of the FP and TM in the membrane and consequently less membrane perturbation. This hypothesis is supported by earlier observations of reduced levels of vesicle fusion for monomer versus trimer hairpin constructs of the HIV gp41 fusion protein.^{47,52,61} gp41 is nonhomologous with HA2, but the two proteins share some structural similarities, including a final hairpin SE state. The reduced level of fusion of the G1E FP of HA2 may also be correlated to shallower membrane insertion of the N-terminal FP.²⁹

Common Enveloped Virus Fusion Model with Significant Functions for Hairpin Trimers and Monomers. We integrate our results and earlier results into a common model for HA-mediated virus/endosome fusion, as well as fusion by other enveloped viruses. The initial trimeric HA1/HA2 complex is the lowest-free energy state at pH 7.4, whereas at pH 5–6 of the mature endosome, the complex is metastable.⁶² The HA1 subunits move away from the HA2 subunits, which then rearrange to the final trimer-of-hairpins state, which is the predominant structural state of WT-HA2 in our experiments. There are accompanying membrane intermediates during fusion that include the hemifusion diaphragm, pore formation, and pore expansion. In some contrast, the HA2 structural intermediates between the initial complex and the final trimer of hairpins have not been experimentally identified. It is sometimes proposed that some of the free energy released during the transformation of HA2 to the final hairpin state is converted to activation energy and perhaps also thermodynamic energy needed for membrane intermediate

states.^{2,4} The pictures usually show a HA2 “prehairpin intermediate” with fully extended SE and with FP inserted in the target membrane that then folds into the final hairpin state, with membrane intermediate formation time-correlated with the evolution of hairpin closure. The final step of fusion pore expansion is sometimes pictured as requiring a transmembrane bundle of three TM segments and sometimes three additional FP segments. The SE hairpin is commonly termed the “postfusion” state, which implies that fusion is completed before the hairpin is formed. This mechanical picture of coupling of HA2 structural changes to lipid rearrangements is visually appealing but is disfavored by the entropic penalties for such a coordinated mechanism.

We propose an alternate model in which FP binds to the target membrane during the HA2 structural transformation to the final hairpin state, and subsequent membrane fusion occurs with HA2 in this final state. The SE hairpin maintains membrane apposition during the ~1 min fusion time, and clustering of hairpin trimers and therefore FP domains in the target membrane perturbs this membrane and lowers the activation barrier to achieving hemifusion and pore formation.^{11,26,47,52} For this model, the SE hairpin is a fusogenic state rather than a postfusion state. This model is supported by WT-HA2-induced vesicle fusion at pH 5.0, which is observed with <100 HA2 trimers per vesicle and fewer than ~400 HA trimers per influenza virion.^{37,38} The SE hairpins may be more stable at pH 5.0 than at pH 7.4, based on the higher T_m for the HA2_{38–89} peptide at pH 5.0 than at pH 7.0, and greater HA2 clustering at low pH is evidenced by visible aggregation of the SE constructs.^{26,43} The fusion relevance of the final hairpin state is also supported by observation of cell/RBC fusion after addition of exogenous FHA2. Such fusion is very similar to HA cell/RBC fusion, with both fusion types requiring low pH and exhibiting nearly identical losses of function for the G1E mutant and for the I173E mutant.^{10,28,63} These mutants also show reduced levels of vesicle fusion (Figure 8). Reduced levels of cell/cell and vesicle fusion for I173E and G1E versus WT proteins correlate with lower SE hairpin stability for the mutants and consequent impaired membrane apposition. There may also be less membrane perturbation by the mutants because of FP binding with the C-terminal strand of the SE and for G1E because of shallower insertion of the FP in the target membrane.

This model can also describe gp41-mediated fusion between the HIV membrane and the plasma membrane of a host cell. gp41 forms an initial trimeric gp160 complex with a receptor-binding protein (gp120) that is analogous with the trimeric HA1/HA2 complex.^{64,65} Fusion occurs via binding of gp120 to host cell receptors, separation of gp120 from gp41, and structural transformation of gp41 into a final trimer-of-hairpins state.^{66,67} A FP+SE+TM gp41 construct in this final state catalyzes fusion at pH 7.4 between vesicles composed of PC and cholesterol or PC, PG, and cholesterol.⁵² This is the pH of HIV/host cell fusion, and there are significant fractions of PC and anionic lipids in the plasma membranes of cells infected by HIV.⁶⁸ gp160 cells also fuse with receptor-bearing cells, and the V2E mutation at the N-terminus of gp41 results in highly impaired V2E versus WT gp160 cell/receptor cell fusion.⁶⁹ This observation correlates with highly impaired G1E- versus WT-HA cell/RBC fusion.

A monomer fraction for HA2 in SEC correlates with monomer fractions of the initial HA1/HA2 complex under some conditions, as well as large monomer fractions for gp41

under some conditions.^{47,48,50,52,56,57,70} For both HA2 and gp41, there is a significant structural rearrangement between the initial trimeric HA1/HA2 or gp160 complex and the final trimer of hairpins without the receptor proteins. Transient dissociation of HA2 and gp41 into monomers may be functionally important because monomer rearrangement into a hairpin followed by association into a trimer of hairpins may be topologically more straightforward than a concerted rearrangement of trimeric protein. Monomer intermediates have also been postulated for the structural transformations of class II and class III enveloped virus fusion proteins.^{3,70} These hypotheses are evidenced by the facts that (1) the initial class II protein complex is a single heterodimer of E1+E2 subunits whereas the final state is a trimer of hairpins of E1 subunits and (2) one class III structure contains two different monomer units, with one monomer similar to the initial state and the other similar to the final state. Monomer gp41 may also be the binding target of peptides that inhibit gp160-mediated fusion and HIV infection and whose sequences correspond to segments of the C-terminal region of the gp41 SE.^{52,63}

SUMMARY

This study reports protein-induced vesicle fusion by the full-length HA2 containing the FP and the TM and a reduced level of fusion by the G1E and I173E mutants. These mutants also result in a reduced level of HA-mediated cell fusion. This study and previous studies support the idea that the HA2 final trimer of hairpins is fusogenic. This implies common features of the influenza virus/endosome fusion and HA2/vesicle fusion, including: (1) apposing the two fusing compartments by folded hairpin HA2 proteins and maintaining this apposition with a stable SE, (2) binding of the FP to the target membrane, and (3) HA2 aggregation at low pH and consequent clustering of membrane-perturbing FP's.

ASSOCIATED CONTENT

Supporting Information

The Supporting Information is available free of charge on the ACS Publications website at DOI: 10.1021/acs.biochem.8b00764.

DNA sequences corresponding to protein inserts and primers, size-exclusion chromatography of replicate samples, SDS-PAGE after cross-linking of replicate samples, CD spectra of replicate samples, CD spectra of I73E-FHA2 with or without 150 mM NaCl and at different protein concentrations, van't Hoff plots, and vesicle fusion for different protein and vesicle preparations (PDF)

AUTHOR INFORMATION

Corresponding Author

*E-mail: weliky@chemistry.msu.edu. Phone: 517-353-1177. Fax: 517-353-1793.

ORCID

David P. Weliky: 0000-0002-2765-5950

Funding

This work was supported by National Institutes of Health Grant R01 AI047153.

Notes

The authors declare no competing financial interest.

ACKNOWLEDGMENTS

The authors acknowledge assistance from the Michigan State University Genomics facility and the use of instrumentation in the Borhan and Lapidus laboratories.

ABBREVIATIONS

CD, circular dichroism; DM, decyl maltoside; DOTAP, 1,2-dioleoyl-3-trimethylammonium propane; DPC, dodecylphosphocholine; FP, fusion peptide; HA, hemagglutinin; IPTG, isopropyl β -D-1-thiogalactopyranoside; LB, Luria-Bertani; N-NBD-DPPE, N-(7-nitro-2,1,3-benzoxadiazol-4-yl) (ammonium salt) dipalmitoylphosphatidylethanolamine; N-Rh-DPPE, N-(lissamine rhodamine B sulfonyl) (ammonium salt) dipalmitoylphosphatidylethanolamine; PAGE, polyacrylamide gel electrophoresis; POPC or PC, 1-palmitoyl-2-oleoyl-*sn*-glycero-3-phosphocholine; POPG or PG, 1-palmitoyl-2-oleoyl-*sn*-glycero-3-[phospho-*rac*-(1-glycerol)] (sodium salt); RBC, red blood cell; SDS, sodium dodecyl sulfate; SE, soluble ectodomain; SEC, size-exclusion chromatography; SRC, N-lauroylsarcosine; TM, transmembrane; WT, wild-type.

REFERENCES

- Fontana, J., and Steven, A. C. (2015) Influenza virus-mediated membrane fusion: Structural insights from electron microscopy. *Arch. Biochem. Biophys.* 581, 86–97.
- White, J. M., Delos, S. E., Brecher, M., and Schornberg, K. (2008) Structures and mechanisms of viral membrane fusion proteins: Multiple variations on a common theme. *Crit. Rev. Biochem. Mol. Biol.* 43, 189–219.
- Kielian, M. (2014) Mechanisms of virus membrane fusion proteins. *Annu. Rev. Virol.* 1, 171–189.
- Harrison, S. C. (2015) Viral membrane fusion. *Virology* 479–480, 498–507.
- Wilson, I. A., Skehel, J. J., and Wiley, D. C. (1981) Structure of the haemagglutinin membrane glycoprotein of influenza virus at 3 Å resolution. *Nature* 289, 366–373.
- Ekiert, D. C., Kashyap, A. K., Steel, J., Rubrum, A., Bhabha, G., Khayat, R., et al. (2012) Cross-neutralization of influenza A viruses mediated by a single antibody loop. *Nature* 489, 526–532.
- Bullough, P. A., Hughson, F. M., Skehel, J. J., and Wiley, D. C. (1994) Structure of influenza haemagglutinin at the pH of membrane fusion. *Nature* 371, 37–43.
- Chen, J., Skehel, J. J., and Wiley, D. C. (1999) N- and C-terminal residues combine in the fusion-pH influenza hemagglutinin HA₂ subunit to form an N cap that terminates the triple-stranded coiled coil. *Proc. Natl. Acad. Sci. U. S. A.* 96, 8967–8972.
- Chernomordik, L. V., Frolov, V. A., Leikina, E., Bronk, P., and Zimmerberg, J. (1998) The pathway of membrane fusion catalyzed by influenza hemagglutinin: Restriction of lipids, hemifusion, and lipid fusion pore formation. *J. Cell Biol.* 140, 1369–1382.
- Qiao, H., Armstrong, R. T., Melikyan, G. B., Cohen, F. S., and White, J. M. (1999) A specific point mutant at position 1 of the influenza hemagglutinin fusion peptide displays a hemifusion phenotype. *Mol. Biol. Cell* 10, 2759–2769.
- Blijleven, J. S., Boonstra, S., Onck, P. R., van der Giessen, E., and van Oijen, A. M. (2016) Mechanisms of influenza viral membrane fusion. *Semin. Cell Dev. Biol.* 60, 78–88.
- Park, H. E., Gruenke, J. A., and White, J. M. (2003) Leash in the groove mechanism of membrane fusion. *Nat. Struct. Mol. Biol.* 10, 1048–1053.
- Borrego-Diaz, E., Peeples, M. E., Markosyan, R. M., Melikyan, G. B., and Cohen, F. S. (2003) Completion of trimeric hairpin formation of influenza virus hemagglutinin promotes fusion pore opening and enlargement. *Virology* 316, 234–244.
- Nobusawa, E., Aoyama, T., Kato, H., Suzuki, Y., Tateno, Y., and Nakajima, K. (1991) Comparison of complete amino acid sequences and receptor binding properties among 13 serotypes of hemagglutinins of influenza A viruses. *Virology* 182, 475–485.
- Cross, K. J., Langley, W. A., Russell, R. J., Skehel, J. J., and Steinhauer, D. A. (2009) Composition and functions of the Influenza fusion peptide. *Protein Pept. Lett.* 16, 766–778.
- Lorieau, J. L., Louis, J. M., and Bax, A. (2010) The complete influenza hemagglutinin fusion domain adopts a tight helical hairpin arrangement at the lipid:water interface. *Proc. Natl. Acad. Sci. U. S. A.* 107, 11341–11346.
- Du, T. P., Jiang, L., and Liu, M. L. (2014) NMR structures of fusion peptide from influenza hemagglutinin H3 subtype and its mutants. *J. Pept. Sci.* 20, 292–297.
- Ghosh, U., Xie, L., and Weliky, D. P. (2013) Detection of closed influenza virus hemagglutinin fusion peptide structures in membranes by backbone ¹³C-¹⁵N rotational-echo double-resonance solid-state NMR. *J. Biomol. NMR* 55, 139–146.
- Ghosh, U., Xie, L., Jia, L. H., Liang, S., and Weliky, D. P. (2015) Closed and semiclosed interhelical structures in membrane vs closed and open structures in detergent for the Influenza Virus hemagglutinin fusion peptide and correlation of hydrophobic surface area with fusion catalysis. *J. Am. Chem. Soc.* 137, 7548–7551.
- Macosko, J. C., Kim, C. H., and Shin, Y. K. (1997) The membrane topology of the fusion peptide region of influenza hemagglutinin determined by spin-labeling EPR. *J. Mol. Biol.* 267, 1139–1148.
- Armstrong, R. T., Kushnir, A. S., and White, J. M. (2000) The transmembrane domain of influenza hemagglutinin exhibits a stringent length requirement to support the hemifusion to fusion transition. *J. Cell Biol.* 151, 425–437.
- Markosyan, R. M., Cohen, F. S., and Melikyan, G. B. (2000) The lipid-anchored ectodomain of influenza virus hemagglutinin (GPI-HA) is capable of inducing nonenlarging fusion pores. *Mol. Biol. Cell* 11, 1143–1152.
- Melikyan, G. B., Lin, S. S., Roth, M. G., and Cohen, F. S. (1999) Amino acid sequence requirements of the transmembrane and cytoplasmic domains of influenza virus hemagglutinin for viable membrane fusion. *Mol. Biol. Cell* 10, 1821–1836.
- Tatullian, S. A., and Tamm, L. K. (2000) Secondary structure, orientation, oligomerization, and lipid interactions of the transmembrane domain of influenza hemagglutinin. *Biochemistry* 39, 496–507.
- Chen, J., Skehel, J. J., and Wiley, D. C. (1998) A polar octapeptide fused to the N-terminal fusion peptide solubilizes the influenza virus HA(2) subunit ectodomain. *Biochemistry* 37, 13643–13649.
- Ratnayake, P. U., Prabodha Ekanayaka, E. A., Komanduru, S. S., and Weliky, D. P. (2016) Full-length trimeric influenza virus hemagglutinin II membrane fusion protein and shorter constructs lacking the fusion peptide or transmembrane domain: Hyperthermostability of the full-length protein and the soluble ectodomain and fusion peptide make significant contributions to fusion of membrane vesicles. *Protein Expression Purif.* 117, 6–16.
- Leikina, E., LeDuc, D. L., Macosko, J. C., Epand, R., Epand, R., Shin, Y. K., and Chernomordik, L. V. (2001) The 1–127 HA₂ construct of influenza virus hemagglutinin induces cell-cell hemifusion. *Biochemistry* 40, 8378–8386.
- Kim, C. S., Epand, R. F., Leikina, E., Epand, R. M., and Chernomordik, L. V. (2011) The final conformation of the complete ectodomain of the HA₂ subunit of Influenza Hemagglutinin can by itself drive low pH-dependent fusion. *J. Biol. Chem.* 286, 13226–13234.
- Wu, C. W., Cheng, S. F., Huang, W. N., Trivedi, V. D., Veeramuthu, B., Kantchev, A. B., Wu, W.-G., and Chang, D.-K. (2003) Effects of alterations of the amino-terminal glycine of influenza hemagglutinin fusion peptide on its structure, organization and membrane interactions. *Biochim. Biophys. Acta, Biomembr.* 1612, 41–51.
- Swalley, S. E., Baker, B. M., Calder, L. J., Harrison, S. C., Skehel, J. J., and Wiley, D. C. (2004) Full-length influenza hemagglutinin HA₂

refolds into the trimeric low-pH-induced conformation. *Biochemistry* 43, 5902–5911.

(31) Curtis-Fisk, J., Spencer, R. M., and Weliky, D. P. (2008) Isotopically labeled expression in *E. coli*, purification, and refolding of the full ectodomain of the Influenza virus membrane fusion protein. *Protein Expression Purif.* 61, 212–219.

(32) Gerl, M. J., Sampaio, J. L., Urban, S., Kalvodova, L., Verbavatz, J. M., Binnington, B., Lindemann, D., Lingwood, C. A., Shevchenko, A., Schroeder, C., and Simons, K. (2012) Quantitative analysis of the lipidomes of the influenza virus envelope and MDCK cell apical membrane. *J. Cell Biol.* 196, 213–221.

(33) Ivanova, P. T., Myers, D. S., Milne, S. B., McClaren, J. L., Thomas, P. G., and Brown, H. A. (2015) Lipid composition of the viral envelope of three strains of Influenza virus—Not all viruses are created equal. *ACS Infect. Dis.* 1, 435–442.

(34) Kobayashi, T., Beuchat, M. H., Chevallier, J., Makino, A., Mayran, N., Escola, J. M., Lebrand, C., Cosson, P., Kobayashi, T., and Gruenberg, J. (2002) Separation and characterization of late endosomal membrane domains. *J. Biol. Chem.* 277, 32157–32164.

(35) Mobius, W., van Donselaar, E., Ohno-Iwashita, Y., Shimada, Y., Heijnen, H. F. G., Slot, J. W., and Geuze, H. J. (2003) Recycling compartments and the internal vesicles of multivesicular bodies harbor most of the cholesterol found in the endocytic pathway. *Traffic* 4, 222–231.

(36) Shangguan, T., Alford, D., and Bentz, J. (1996) Influenza-virus-liposome lipid mixing is leaky and largely insensitive to the material properties of the target membrane. *Biochemistry* 35, 4956–4965.

(37) Harris, A., Cardone, G., Winkler, D. C., Heymann, J. B., Brecher, M., White, J. M., and Steven, A. C. (2006) Influenza virus pleiomorphy characterized by cryoelectron tomography. *Proc. Natl. Acad. Sci. U. S. A.* 103, 19123–19127.

(38) Yamaguchi, M., Danev, R., Nishiyama, K., Sugawara, K., and Nagayama, K. (2008) Zernike phase contrast electron microscopy of ice-embedded influenza A virus. *J. Struct. Biol.* 162, 271–276.

(39) Eband, R. F., Macosko, J. C., Russell, C. J., Shin, Y. K., and Eband, R. M. (1999) The ectodomain of HA2 of influenza virus promotes rapid pH dependent membrane fusion. *J. Mol. Biol.* 286, 489–503.

(40) Yang, J., Gabrys, C. M., and Weliky, D. P. (2001) Solid-state nuclear magnetic resonance evidence for an extended beta strand conformation of the membrane-bound HIV-1 fusion peptide. *Biochemistry* 40, 8126–8137.

(41) Curtis-Fisk, J., Preston, C., Zheng, Z. X., Worden, R. M., and Weliky, D. P. (2007) Solid-state NMR structural measurements on the membrane-associated influenza fusion protein ectodomain. *J. Am. Chem. Soc.* 129, 11320–11321.

(42) Durrer, P., Galli, C., Hoenke, S., Corti, C., Gluck, R., Vorherr, T., and Brunner, J. (1996) H⁺-induced membrane insertion of influenza virus hemagglutinin involves the HA2 amino-terminal fusion peptide but not the coiled coil region. *J. Biol. Chem.* 271, 13417–13421.

(43) Carr, C. M., and Kim, P. S. (1993) A spring-loaded mechanism for the conformational change of influenza hemagglutinin. *Cell* 73, 823–832.

(44) Kim, C. H., Macosko, J. C., Yu, Y. G., and Shin, Y. K. (1996) On the dynamics and confirmation of the HA2 domain of the influenza virus hemagglutinin. *Biochemistry* 35, 5359–5365.

(45) Lorieau, J. L., Louis, J. M., and Bax, A. (2011) Helical hairpin structure of Influenza Hemagglutinin fusion peptide stabilized by charge-dipole interactions between the N-terminal amino group and the second helix. *J. Am. Chem. Soc.* 133, 2824–2827.

(46) Murphy, K. P., and Freire, E. (1992) Thermodynamics of structural stability and cooperative folding behavior in proteins. *Adv. Protein Chem.* 43, 313–361.

(47) Banerjee, K., and Weliky, D. P. (2014) Folded monomers and hexamers of the ectodomain of the HIV gp41 membrane fusion protein: Potential roles in fusion and synergy between the fusion peptide, hairpin, and membrane-proximal external region. *Biochemistry* 53, 7184–7198.

(48) Roche, J., Louis, J. M., Grishaev, A., Ying, J. F., and Bax, A. (2014) Dissociation of the trimeric gp41 ectodomain at the lipid-water interface suggests an active role in HIV-1 Env-mediated membrane fusion. *Proc. Natl. Acad. Sci. U. S. A.* 111, 3425–3430.

(49) Cho, K. J., Lee, J.-H., Hong, K. W., Kim, S.-H., Park, Y., Lee, J. Y., and Kim, K. H. (2013) Insight into structural diversity of influenza virus haemagglutinin. *J. Gen. Virol.* 94, 1712–1722.

(50) Dai, Z., Tao, Y. S., Liu, N. N., Brenowitz, M. D., Girvin, M. E., and Lai, J. R. (2015) Conditional trimerization and lytic activity of HIV-1 gp41 variants containing the membrane-associated segments. *Biochemistry* 54, 1589–1599.

(51) Joyce, M. G., Wheatley, A. K., Thomas, P. V., Chuang, G.-Y., Soto, C., Bailer, R. T., et al. (2016) Vaccine-induced antibodies that neutralize group 1 and group 2 Influenza A viruses. *Cell* 166, 609–623.

(52) Liang, S., Ratnayake, P. U., Keinath, C., Jia, L., Wolfe, R., Ranaweera, A., and Weliky, D. P. (2018) Efficient fusion at neutral pH by Human Immunodeficiency Virus gp41 trimers containing the fusion peptide and transmembrane domains. *Biochemistry* 57, 1219–1235.

(53) Xiong, X., Corti, D., Liu, J., Pinna, D., Foglierini, M., Calder, L. J., Martin, S. R., Lin, Y. P., Walker, P. A., Collins, P. J., Monne, I., Suguitan, A. L., Santos, C., Temperton, N. J., Subbarao, K., Lanzavecchia, A., Gamblin, S. J., and Skehel, J. J. (2015) Structures of complexes formed by H5 influenza hemagglutinin with a potent broadly neutralizing human monoclonal antibody. *Proc. Natl. Acad. Sci. U. S. A.* 112, 9430–9435.

(54) Seok, J. H., Kim, J., Lee, D. B., Cho, K. J., Lee, J.-H., Bae, G., Chung, M. S., and Kim, K. H. (2017) Conformational modulation of influenza virus hemagglutinin: characterization and in vivo efficacy of monomeric form. *Sci. Rep.* 7, 7540.

(55) Raymond, D. D., Stewart, S. M., Lee, J., Ferdman, J., Bajic, G., Do, K. T., Harrison, S. C., et al. (2016) Influenza immunization elicits antibodies specific for an egg-adapted vaccine strain. *Nat. Med.* 22, 1465.

(56) Lakomek, N. A., Kaufman, J. D., Stahl, S. J., Louis, J. M., Grishaev, A., Wingfield, P. T., and Bax, A. (2013) Internal dynamics of the homotrimeric HIV-1 viral coat protein gp41 on multiple time scales. *Angew. Chem., Int. Ed.* 52, 3911–3915.

(57) Chiliveri, S. C., Louis, J. M., Ghirlando, R., Baber, J. L., and Bax, A. (2018) Tilted, uninterrupted, monomeric HIV-1 gp41 transmembrane helix from residual dipolar couplings. *J. Am. Chem. Soc.* 140, 34–37.

(58) Balakrishnan, K., Krishnan, N. M., and Rao, B. J. (2009) Salt modulates oligomerization properties of hRad51 and hRad52 proteins. *Open Biol.* 2, 1–9.

(59) Politi, L., Chiancone, E., Giangiacomo, L., Cervoni, L., Scotto D'Abusco, A., Scorsino, S., and Scandurra, R. (2009) pH-, temperature- and ion-dependent oligomerization of *Sulfolobus solfataricus* recombinant amidase: a study with site-specific mutants. *Archaea* 2, 221–231.

(60) Zawada, K. E., Okamoto, K., and Kasson, P. M. (2018) Influenza hemifusion phenotype depends on membrane context: Differences in cell-cell and virus-cell fusion. *J. Mol. Biol.* 430, 594–601.

(61) Ratnayake, P. U., Sackett, K., Nethercott, M. J., and Weliky, D. P. (2015) pH-dependent vesicle fusion induced by the ectodomain of the human immunodeficiency virus membrane fusion protein gp41: Two kinetically distinct processes and fully-membrane-associated gp41 with predominant beta sheet fusion peptide conformation. *Biochim. Biophys. Acta, Biomembr.* 1848, 289–298.

(62) Eband, R. F., and Eband, R. M. (2003) Irreversible unfolding of the neutral pH form of influenza hemagglutinin demonstrates that it is not in a metastable state. *Biochemistry* 42, 5052–5057.

(63) Markosyan, R. M., Cohen, F. S., and Melikyan, G. B. (2003) HIV-1 envelope proteins complete their folding into six-helix bundles immediately after fusion pore formation. *Mol. Biol. Cell* 14, 926–938.

- (64) Pancera, M., Zhou, T. Q., Druz, A., Georgiev, I. S., Soto, C., Gorman, J., Kwong, P. D., et al. (2014) Structure and immune recognition of trimeric pre-fusion HIV-1 Env. *Nature* 514, 455–461.
- (65) Garces, F., Lee, J. H., de Val, N., Torrents de la Pena, A., Kong, L., Puchades, C., Hua, Y., Stanfield, R. L., Burton, D. R., Moore, J. P., Sanders, R. W., Ward, A. B., and Wilson, I. A. (2015) Affinity maturation of a potent family of HIV antibodies is primarily focused on accommodating or avoiding glycans. *Immunity* 43, 1053–1063.
- (66) Caffrey, M., Cai, M., Kaufman, J., Stahl, S. J., Wingfield, P. T., Covell, D. G., and Clore, G. M. (1998) Three-dimensional solution structure of the 44 kDa ectodomain of SIV gp41. *EMBO J.* 17, 4572–4584.
- (67) Yang, Z. N., Mueser, T. C., Kaufman, J., Stahl, S. J., Wingfield, P. T., and Hyde, C. C. (1999) The crystal structure of the SIV gp41 ectodomain at 1.47 Å resolution. *J. Struct. Biol.* 126, 131–144.
- (68) Lorizate, M., Sachsenheimer, T., Glass, B., Habermann, A., Gerl, M. J., Krausslich, H. G., and Brugger, B. (2013) Comparative lipidomics analysis of HIV-1 particles and their producer cell membrane in different cell lines. *Cell. Microbiol.* 15, 292–304.
- (69) Freed, E. O., Delwart, E. L., Buchschacher, G. L., Jr., and Panganiban, A. T. (1992) A mutation in the human immunodeficiency virus type 1 transmembrane glycoprotein gp41 dominantly interferes with fusion and infectivity. *Proc. Natl. Acad. Sci. U. S. A.* 89, 70–74.
- (70) Abou-Hamdan, A., Belot, L., Albertini, A., and Gaudin, Y. (2018) Monomeric intermediates formed by Vesiculovirus glycoprotein during its low-pH-induced structural transition. *J. Mol. Biol.* 430, 1685–1695.

Supplementary Information for “Stabilities of the Soluble Ectodomain and Fusion Peptide Hairpins of the Influenza Virus Hemagglutinin Subunit II Protein Are Positively-Correlated with Membrane Fusion”

Ahinsa Ranaweera, Punsisi Upeka Ratnayake, and David Paul Weliky*

Department of Chemistry, Michigan State University, East Lansing, MI 48824 USA

Figure S1. DNA sequences of FHA2 and HA2 constructs. Each line is 60 nucleotides. Bold nucleotides correspond to residues 1 and 173.

FHA2

GGTCTGTTCGGTGCTATCGCTGGCTTTATTGAAAATGGCTGGGAAGGCATGATTGATGGC
TGGTACGGCTTTCGTCACCAAACTCGGAAGGCACCGGTCAGGCGGCGGATCTGAAAAGC
ACGCAGGCAGCTATTGACCAAATCAACGGCAAACCTGAATCGTGTTCATCGAAAAACCAAC
GAAAAATTCATCAGATCGAAAAAGAATTTAGCGAAGTGGAAGGTCGCATTCAAGATCTG
GAAAAATACGTTCGAAGATACGAAAATCGACCTGTGGAGTTACAACGCAGAACTGCTGGTT
GCGCTGGAAAATCAGCACACCATTGATCTGACGGACTCCGAAATGAACAACTGTTTCGAA
AAAACCCGTCGCCAACTGCGTGAAAACGCAGAAGAAATGGGCAATGGTAGCTTCAAATC
TATCATAAAGCCGATAACGCGGCCATTCGCTCTATCCGCAATGGCACGTATGATCACGC
GTTTACCGCGACGAAGCCCTGAACAATCGCTTCCAA**ATC**AAAGGTGTGCGAACTGAAAAGT
GGCTACAAAGACTGGCTCGAGCACCACCACCACCAC

G1E – FHA2

GAGCTGTTCGGTGCTATCGCTGGCTTTATTGAAAATGGCTGGGAAGGCATGATTGATGGC
TGGTACGGCTTTCGTCACCAAACTCGGAAGGCACCGGTCAGGCGGCGGATCTGAAAAGC
ACGCAGGCAGCTATTGACCAAATCAACGGCAAACCTGAATCGTGTTCATCGAAAAACCAAC
GAAAAATTCATCAGATCGAAAAAGAATTTAGCGAAGTGGAAGGTCGCATTCAAGATCTG
GAAAAATACGTTCGAAGATACGAAAATCGACCTGTGGAGTTACAACGCAGAACTGCTGGTT
GCGCTGGAAAATCAGCACACCATTGATCTGACGGACTCCGAAATGAACAACTGTTTCGAA
AAAACCCGTCGCCAACTGCGTGAAAACGCAGAAGAAATGGGCAATGGTAGCTTCAAATC
TATCATAAAGCCGATAACGCGGCCATTCGCTCTATCCGCAATGGCACGTATGATCACGC
GTTTACCGCGACGAAGCCCTGAACAATCGCTTCCAA**ATC**AAAGGTGTGCGAACTGAAAAGT
GGCTACAAAGACTGGCTCGAGCACCACCACCACCAC

I173E-FHA2

GGTCTGTTCGGTGCTATCGCTGGCTTTATTGAAAATGGCTGGGAAGGCATGATTGATGGC
TGGTACGGCTTTCGTCACCAAACTCGGAAGGCACCGGTCAGGCGGCGGATCTGAAAAGC
ACGCAGGCAGCTATTGACCAAATCAACGGCAAACCTGAATCGTGTTCATCGAAAAACCAAC
GAAAAATTCATCAGATCGAAAAAGAATTTAGCGAAGTGGAAGGTCGCATTCAAGATCTG
GAAAAATACGTTCGAAGATACGAAAATCGACCTGTGGAGTTACAACGCAGAACTGCTGGTT
GCGCTGGAAAATCAGCACACCATTGATCTGACGGACTCCGAAATGAACAACTGTTTCGAA
AAAACCCGTCGCCAACTGCGTGAAAACGCAGAAGAAATGGGCAATGGTAGCTTCAAATC
TATCATAAAGCCGATAACGCGGCCATTCGCTCTATCCGCAATGGCACGTATGATCACGC
GTTTACCGCGACGAAGCCCTGAACAATCGCTTCCAA**GAG**AAAGGTGTGCGAACTGAAAAGT
GGCTACAAAGACTGGCTCGAGCACCACCACCACCAC

HA2

GGTCTGTTCCGGTGCTATCGCTGGCTTTATTGAAAACGGTTGGGAAGGCATGATCGACGGC
TGGTACGGCTTTTCGCCATCAAAACTCAGAAGGCACCGGTCAGGCGGCGGATCTGAAAAGC
ACGCAGGCAGCTATTGACCAAATCAACGGCAAACCTGAATCGTGTGATCGAAAAACCAAC
GAAAAATTCATCAGATCGAAAAAGAATTTTCTGAAGTCGAAGGTCGCATTCAAGATCTG
GAAAAATATGTGGAAGATACGAAAATCGACCTGTGGTCATACAACGCGGAACTGCTGGTT
GCCCTGGAAAATCAGCACACCATTTGATCTGACGGACTCGGAAATGAACAACTGTTTCGAA
AAAACCCGTCGCCAACTGCGTGAAAACGCAGAAGAAATGGGCAACGGTAGTTTCAAATC
TACCATAAAGCTGATAACGCGGCCATTGAATCCATCCGCAATGGCACGTATGATCACGAC
GTTTACCGTGACGAAGCGCTGAACAATCGCTTTCAG**ATT**AAAGGCGTCGAACTGAAATCC
GGTTACAAAGATTGGATTCTGTGGATCAGCTTTGCAATTTCTGCTTTCCTGCTGGCCGTG
GTTCTGCTGGGTTTTCATCATGTGGGCGGCGCAGCGTGGCAACATTCGTGCAAACATCGCA
ATCGGTGGCGGTGGCGGGCGGCTCGAGCACCACCACCACCACCAC

G1E-HA2

GAGCTGTTCCGGTGCTATCGCTGGCTTTATTGAAAACGGTTGGGAAGGCATGATCGACGGC
TGGTACGGCTTTTCGCCATCAAAACTCAGAAGGCACCGGTCAGGCGGCGGATCTGAAAAGC
ACGCAGGCAGCTATTGACCAAATCAACGGCAAACCTGAATCGTGTGATCGAAAAACCAAC
GAAAAATTCATCAGATCGAAAAAGAATTTTCTGAAGTCGAAGGTCGCATTCAAGATCTG
GAAAAATATGTGGAAGATACGAAAATCGACCTGTGGTCATACAACGCGGAACTGCTGGTT
GCCCTGGAAAATCAGCACACCATTTGATCTGACGGACTCGGAAATGAACAACTGTTTCGAA
AAAACCCGTCGCCAACTGCGTGAAAACGCAGAAGAAATGGGCAACGGTAGTTTCAAATC
TACCATAAAGCTGATAACGCGGCCATTGAATCCATCCGCAATGGCACGTATGATCACGAC
GTTTACCGTGACGAAGCGCTGAACAATCGCTTTCAG**ATT**AAAGGCGTCGAACTGAAATCC
GGTTACAAAGATTGGATTCTGTGGATCAGCTTTGCAATTTCTGCTTTCCTGCTGGCCGTG
GTTCTGCTGGGTTTTCATCATGTGGGCGGCGCAGCGTGGCAACATTCGTGCAAACATCGCA
ATCGGTGGCGGTGGCGGGCGGCTCGAGCACCACCACCACCACCAC

I173E-HA2

GGTCTGTTCCGGTGCTATCGCTGGCTTTATTGAAAACGGTTGGGAAGGCATGATCGACGGC
TGGTACGGCTTTTCGCCATCAAAACTCAGAAGGCACCGGTCAGGCGGCGGATCTGAAAAGC
ACGCAGGCAGCTATTGACCAAATCAACGGCAAACCTGAATCGTGTGATCGAAAAACCAAC
GAAAAATTCATCAGATCGAAAAAGAATTTTCTGAAGTCGAAGGTCGCATTCAAGATCTG
GAAAAATATGTGGAAGATACGAAAATCGACCTGTGGTCATACAACGCGGAACTGCTGGTT
GCCCTGGAAAATCAGCACACCATTTGATCTGACGGACTCGGAAATGAACAACTGTTTCGAA
AAAACCCGTCGCCAACTGCGTGAAAACGCAGAAGAAATGGGCAACGGTAGTTTCAAATC
TACCATAAAGCTGATAACGCGGCCATTGAATCCATCCGCAATGGCACGTATGATCACGAC
GTTTACCGTGACGAAGCGCTGAACAATCGCTTTCAG**GAG**AAAGGCGTCGAACTGAAATCC
GGTTACAAAGATTGGATTCTGTGGATCAGCTTTGCAATTTCTGCTTTCCTGCTGGCCGTG
GTTCTGCTGGGTTTTCATCATGTGGGCGGCGCAGCGTGGCAACATTCGTGCAAACATCGCA
ATCGGTGGCGGTGGCGGGCGGCTCGAGCACCACCACCACCACCAC

Figure S2. Primer sequences to produce mutants.

G1E -FHA2 and -HA2 forward

5' – CAT ATG GAG CTG TTC GGT GC – 3'

G1E -FHA2 and -HA2 reverse

5' – GCA CCG AAC AGC TCC ATA TG – 3'

I173E-FHA2 forward

5' – CGC TTC CAA GAG AAA GGT GTC – 3'

I173E-FHA2 reverse

5' – GAC ACC TTT CTC TTG GAA GCG – 3'

I173E-HA2 forward

5' – CGC TTT CAG GAG AAA GGC GTC – 3'

I173E-HA2 reverse

5' – GAC GCC TTT CTC CTG AAA GCG – 3'

Figure S3. SEC traces prior to cross-linking (left) of replicate samples and SDS-PAGE after cross-linking (right) of replicate samples and in (A) SRC and (B) DM detergents (compare to Fig. 3).

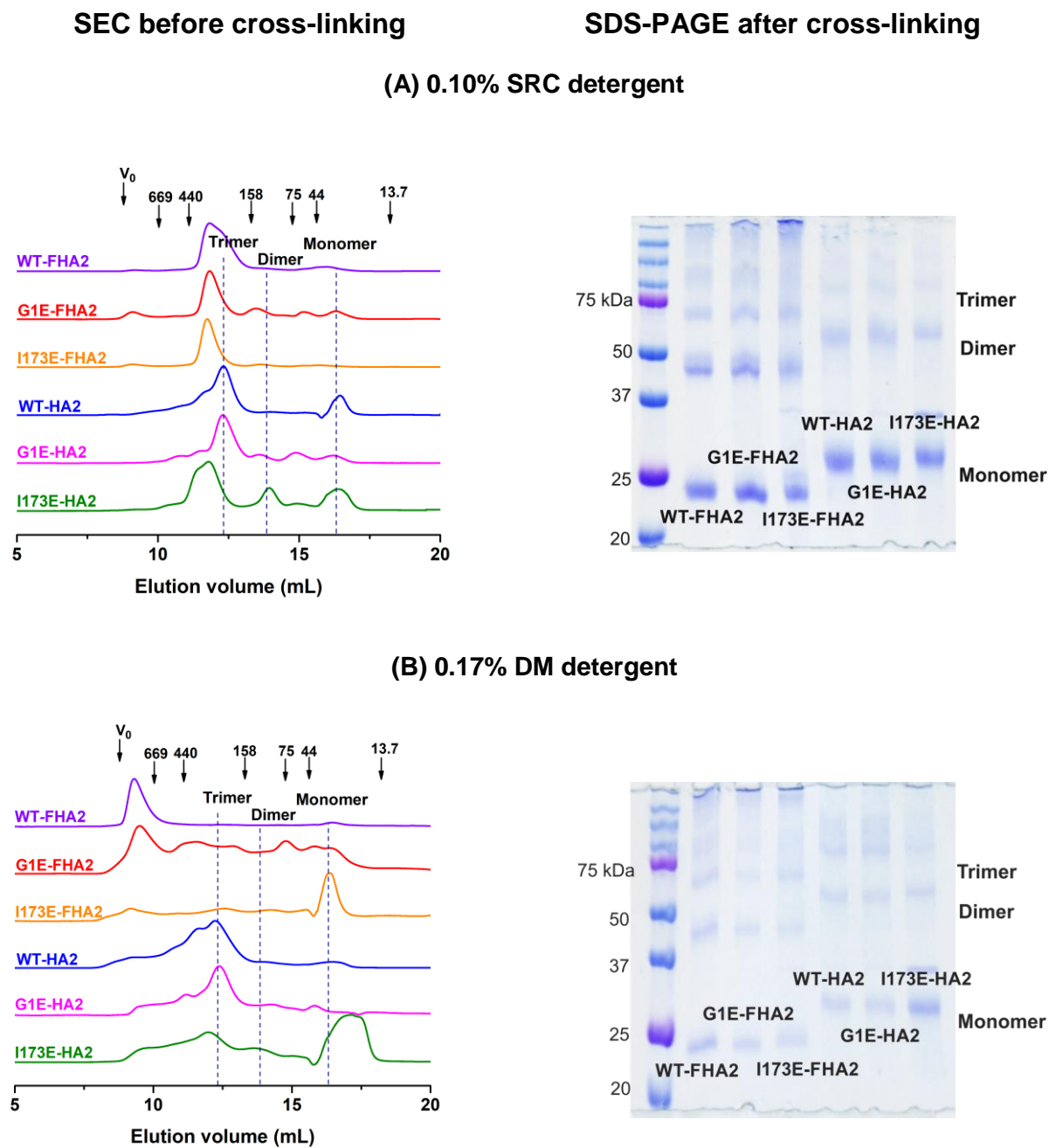
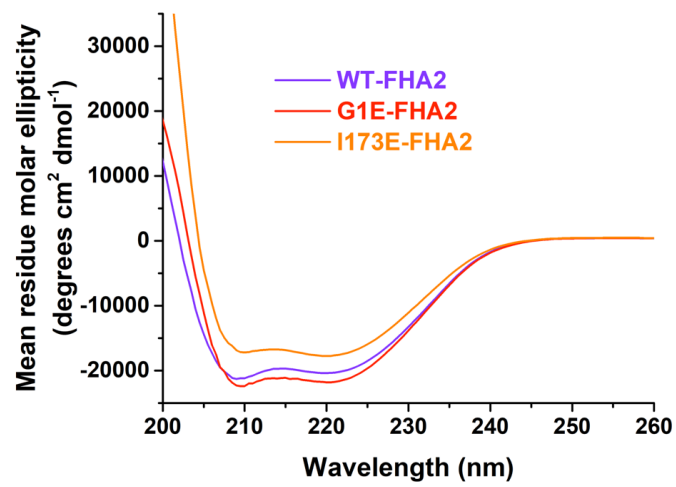


Figure S4. CD spectra of replicates samples (compare to Fig. 4).

(A) FHA2



(B) HA2

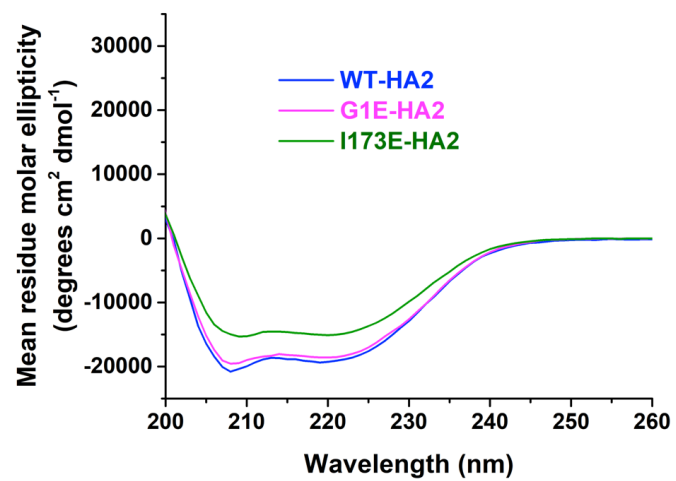


Figure S5. Comparison of ambient-temperature CD spectra of I173E-FHA2 without or with 150 mM NaCl. The buffers also contained 10 mM Tris-HCl at pH 7.4 and 0.17% DM. Samples were prepared by diluting protein stock solution into buffer without or with 150 mM NaCl. The larger $|\theta_{222}|$ values for $[I173E-FHA2] = 1 \mu\text{M}$ vs. higher protein concentrations likely reflect error in the $1 \mu\text{M}$ concentration.

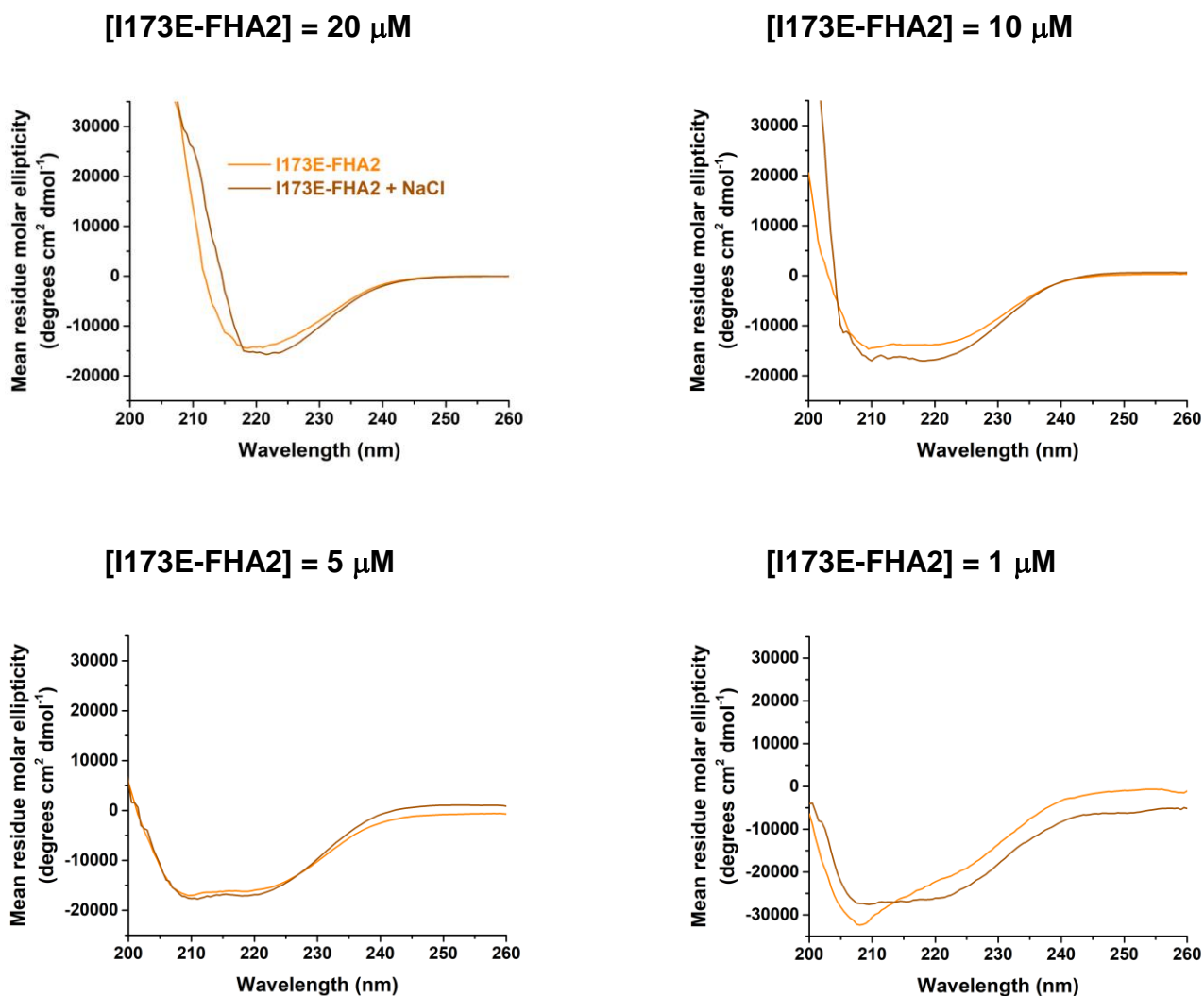


Figure S6. van't Hoff plots of the unfolding $\ln K_{eq}$ vs. $1/T$ based on θ_{222} data for the temperature range around T_m . Best-fit parameters are given with uncertainties in parentheses.

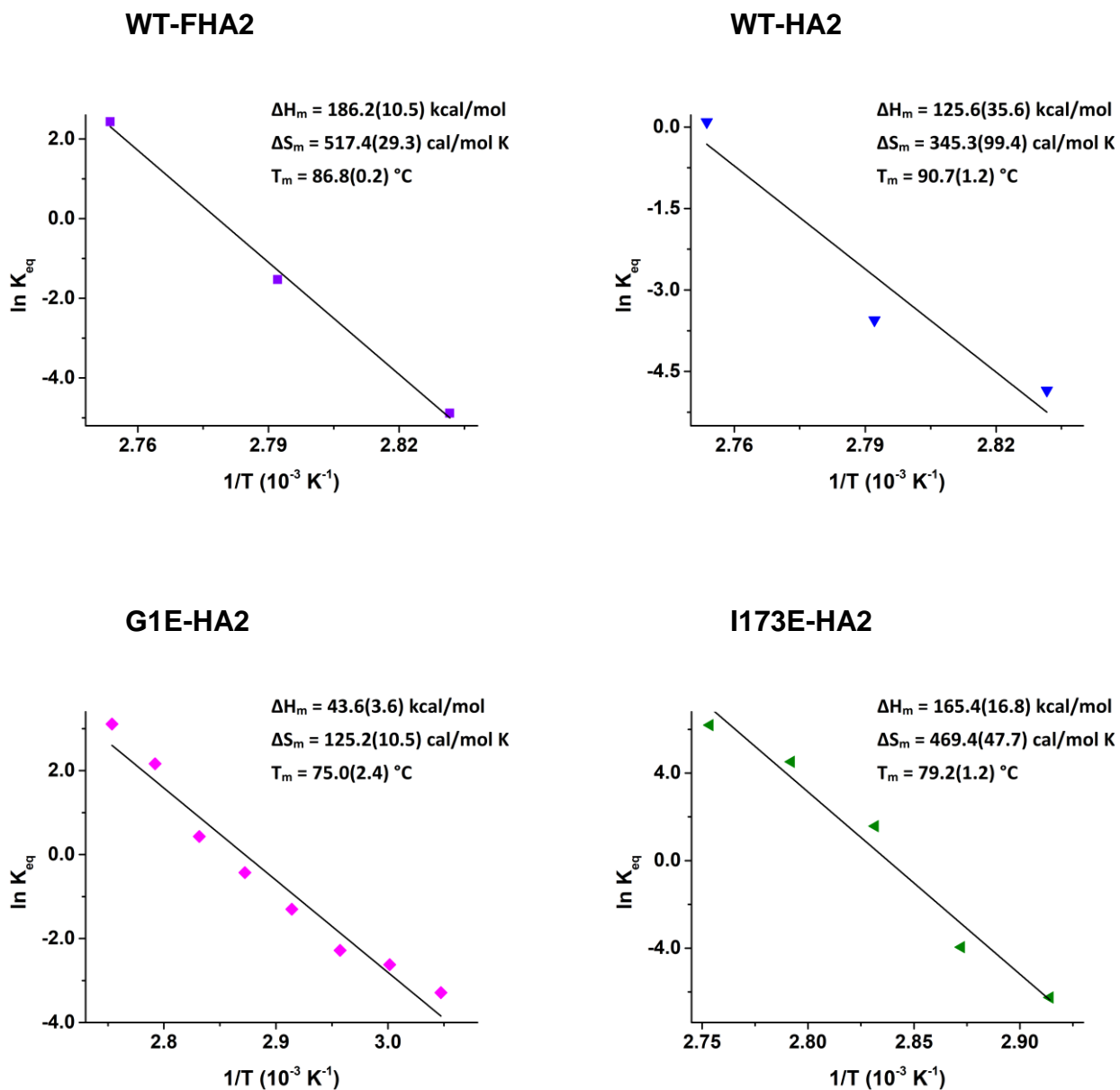


Figure S7. Extents of HA2-induced vesicle fusion using different preparations of proteins and vesicles (compare to Fig. 8B).

